Magnetically dressed one-electron molecular orbitals

Uwe Wille
Bereich Kern- und Strahlenphysik, Hahn-Meitner-Institut Berlin, Postfach 39 01 28, D-1000 Berlin 39, West Germany
(Received 25 April 1988)

A general method for solving the stationary one-electron, two-center Coulomb problem with a superimposed (uniform) strong magnetic field is described and applied. For arbitrary orientation of the field with respect to the line connecting the centers, the pertinent Schrödinger equation is solved by evaluating analytically the Hamiltonian matrix in a basis of (nonorthogonal) Hylleraas functions and solving numerically the generalized eigenvalue problem for this matrix. A detailed study of the properties of "magnetically dressed" (diatomic) one-electron molecular orbitals is performed by calculating energies and wave functions for the H_2^+ and $(H\text{-}He)^{2+}$ systems for field strengths up to about 10^8 T. Molecular-orbital correlation diagrams are presented and discussed, in which dressed-orbital energies are displayed as a function of internuclear distance R at fixed angle θ between field direction and internuclear axis, and as a function of θ at fixed R. Equilibrium internuclear distances and total binding energies are calculated as functions of field strength for the magnetically dressed H_2^+ system in its lowest gerade and ungerade states at $\theta=0$ and $\theta=90°$. The influence of the magnetic field on molecular binding properties as well as on the separation behavior of molecular orbitals at large internuclear distances is illustrated by means of wave-function plots. Whenever possible, our results are compared to those of previous investigations. The convergence properties of our method are discussed.

I. INTRODUCTION

The structure and dynamics of atomic systems exposed to strong, external (static) magnetic fields have recently attracted great interest. By definition, strong fields are characterized[1,2] by magnetic interaction energies which are comparable to, or larger than, typical Coulombic energies in the unperturbed system, i.e., by field strengths substantially larger than those characteristic of the linear Zeeman effect and of the Paschen-Back effect.

A great deal of motivation for studying the effect of strong magnetic fields on atomic systems has arisen from the established existence[1,3,4] of very strong magnetic fields in the vicinity of degenerate astrophysical objects, with field strengths B estimated to be of order 10^2-10^5 T for white-dwarf stars and 10^7-10^9 T for neutron stars. Fields of this magnitude are capable of considerably modifying or even completely changing the properties of ground states and low-lying excited states of atoms and molecules, as is seen by comparing their strength to the "critical" field strength $B_0=2.35\times10^5$ T at which the oscillator energy associated with the field is equal to the ground-state binding energy of the hydrogen atom. Further impetus to the study of strong-field effects has been provided[5-7] in recent years by the possibility of preparing atomic systems in well-defined, highly excited Rydberg states. These states are strongly perturbed already by magnetic fields easily accessible in the laboratory. Some interest in the general properties of atomic systems exposed to strong magnetic fields has been advanced also in solid-state physics.[1,8,9] Aside from the interest in strong-field studies arising in conjunction with specific applications, there is a general interest in the theoretical study[10,11] of simple atomic systems in strong magnetic fields. These systems may serve as prototype systems for investigating the consequences of nonseparability in (classical or quantum) Hamiltonian systems; in particular, the transition from regular to irregular motion.[11]

Theoretical investigations dealing with effects of strong magnetic fields have been restricted so far essentially to the study of bound-state properties of the simplest atomic and molecular systems, viz., the hydrogen atom and the hydrogen molecular ion. The study of continuum properties[12-14] and of scattering processes[14,15] appears to be still in its infancy.

Many authors (see Ref. 16 and references cited therein) have calculated properties of the "magnetically dressed" hydrogen atom by solving, within different approximation schemes, the pertinent Schrödinger equation with the diamagnetic interaction term included in the Hamiltonian. In the most advanced of these calculations, the Hamiltonian is diagonalized in a space of suitably chosen basis functions with a dimension so large that converged results are obtained for energies and wave functions. Extensive tabulations of highly accurate energy eigenvalues of the magnetically dressed hydrogen atom for field strengths up to about 10^9 T can be found in Ref. 16. The associated wave functions have been used in Ref. 17 to calculate oscillator strengths and probabilities of electromagnetic transitions. Recent large-scale calculations[18,19] for magnetically dressed hydrogen Rydberg states have given indications for the onset of irregularities ("quantum chaos") in the photoabsorption spectra, which have been verified experimentally[20] at $B=6$ T.

The influence of strong magnetic fields on the properties of (diatomic) molecular systems, which is the subject

of the present paper, has been discussed first by Kadomtsev and Kudryavtsev.[21] Subsequently, a variety of detailed calculations[22–40] has been performed, which has almost exclusively dealt with the simplest molecular system, viz., the hydrogen molecular ion H_2^+. For fixed internuclear separation, approximate solutions of the Schrödinger equation describing the motion of one electron exposed to the Coulomb fields of two protons and to a strong magnetic field were obtained mainly by means of variational techniques.

In the first such calculation, de Melo *et al.*[22] have assumed the field to be parallel to the internuclear axis and have studied properties of the magnetically dressed H_2^+ system in its electronic $1\sigma_g$ ground state. The trial wave function used by de Melo *et al.* is a product of the lowest Landau orbital corresponding to the actual field strength B and of a single-parameter function describing the motion in the direction parallel to the magnetic field. This specific form of wave function is expected to give accurate results in the range of very strong fields ($B > 10^6$ T). The calculations of de Melo *et al.* were extended up to $B = 10^{10}$ T and established quantitatively that, while the equilibrium internuclear separation of the H_2^+ ground state decreases with increasing field strength, the binding energy and the frequency of vibrations about the equilibrium position increase. Lai[24] has improved the calculations of de Melo *et al.* and extended them to lower field strengths by allowing the range parameter in the Landau orbital to be an additional variational parameter. A four-parameter trial wave function (including the internuclear distance as a variational parameter) adapted to the high-field regime was employed by Warke and Dutta[26] in a calculation of equilibrium binding energies of the H_2^+ system in the $1\sigma_g$ and $1\pi_u$ states.

Variational calculations on the magnetically dressed H_2^+ system based on trial wave functions adapted specifically to the low-field regime have first been performed by Lai and Suen.[23] To study the $1\sigma_g$ state, they used one-parameter as well as three-parameter trial wave functions constructed from hydrogenic $1s$ and $2s$ wave functions centered about the protons in the H_2^+ ion. Similar wave functions have been adopted by de Melo *et al.*[27] Ozaki and Tomishima[32] employed a two-parameter trial wave function constructed from hydrogenic functions to study the $1\sigma_g$ and $1\pi_u$ states; the $1\pi_u$ state was found to become bonding at a field strength $B \approx B_0/10$. The low-field regime was particularly emphasized in the variational calculations of Peek and Katriel[29] who used the most general function separable in prolate spheroidal coordinates as a trial wave function, thereby assuring that the zero-field limit is treated exactly.

Larsen[33] has been the first to treat, within a variational approach, the magnetically dressed H_2^+ system for the case where the field is inclined with respect to the internuclear axis by an arbitrary, nonzero angle θ. In this case, the orbital angular momentum component along the internuclear axis is no longer a good quantum number. Larsen calculated, in particular, frequencies of transverse vibrations (i.e., vibrations perpendicular to the field direction) of the H_2^+ system in its electronic ground state for $B \leq 10^3 B_0$. Khersonskij[36,37,39] used a variational approach to calculate the H_2^+ ground-state energy as a function of internuclear distance and of the angle θ for B values ranging between 10^7 and 10^9 T.

A number of methods other than the pure variational method have been applied to study the magnetically dressed H_2^+ system for the case where the field is parallel to the internuclear axis. Bhaduri *et al.*[25] assumed a universal dependence of the wave function on a single variable depending in a prescribed manner on the electronic coordinates and determined the functional form of the wave function by solving a one-dimensional (Schrödinger-like) differential equation. Kaschiev *et al.*[30] used the finite-element method, while Ozaki and Tomishima[31] employed Monte-Carlo techniques to solve the Schrödinger equation. In the approach of Wunner *et al.*[34] ("adiabatic approximation"), the wave function is written as a product of a Landau orbital corresponding to the actual field strength and an arbitrary function describing the motion in the direction parallel to the magnetic field; the latter function is determined by solving a one-dimensional differential equation. Le Guillou and Zinn-Justin[38] have generalized the adiabatic approximation by treating the range parameter of the Landau orbital as a variational parameter. Vincke and Baye[40] have diagonalized the Hamiltonian of the magnetically dressed H_2^+ system in a basis of functions having Gaussian behavior perpendicular to the field and exponential behavior in the direction parallel to the field. The values of the parameters entering the basis functions were fixed *a priori*. The calculations of Vincke and Baye include states with orbital angular momentum projection $0, -1, \ldots, -4$ for field strengths ranging between $10B_0$ and $10^3 B_0$.

Attempts to study the influence of strong magnetic fields on diatomic molecular systems other than the H_2^+ system have been made in a few cases. Zaucer and Azman[28] have applied a Hartree-Fock–type approach to the H_2 and LiH systems, while Turbiner[35(a)] and Basile *et al.*[35(b)] used variational methods to treat the H_2 system.

In the present paper, we describe and apply a general method for calculating magnetically dressed one-electron molecular orbitals. Our method is based upon an expansion of the Schrödinger wave function in terms of (nonorthogonal) basis functions of the Hylleraas form,[41] which contain a single parameter whose value is fixed *a priori*. The solution of the Schrödinger equation for a given set of symmetry quantum numbers is thereby reduced to the solution of a generalized eigenvalue problem for the corresponding Hamiltonian matrix. In principle, this method allows the immediate calculation of any bound state of the magnetically dressed system at arbitrary values of the external parameters (i.e., of nuclear charge numbers, field strength, internuclear distance, and angle between field direction and internuclear axis), and is therefore more flexible than variational methods which usually require an *ad hoc* construction of a trial wave function for each state separately. The basis expansion method we use has the clear advantage that the convergence of the results can be assessed by performing se-

quences of calculations with progressively larger basis size. The limitations of the method are determined essentially by the limits set by computer storage and computing time.

The principal aim of this paper is to investigate, in a broad range of the external parameters, general properties of magnetically dressed one-electron molecular orbitals, such as orbital energies and wave functions, total binding energies, and equilibrium internuclear distances. Specifically, we are interested in the behavior of the dressed orbitals at large internuclear separations R and in their dependence on the angle θ between field direction and internuclear axis. Most of the previous studies have only marginally considered these cases. The knowledge of the large-R behavior and of the full θ dependence is prerequisite to the study of vibrational and rotational properties of magnetically dressed molecules and to the quasimolecular treatment of (slow) ion-atom collisions proceeding in the presence of a strong magnetic field.

The organization of the paper is as follows. In Sec. II, we set up the Hamiltonian for the nonrelativistic two-center Coulomb problem with superimposed strong magnetic field, and discuss some general properties of this Hamiltonian. In Sec. III, we discuss the properties of the Hylleraas basis functions and describe the diagonalization procedure used to solve the Schrödinger equation. Section IV is devoted to the study of properties of magnetically dressed one-electron molecular orbitals for the case that the field direction is parallel to the internuclear axis. The general case of an arbitrary angle between field direction and internuclear axis is considered in Sec. V. Section VI summarizes the contents of the paper and presents our conclusions. Brief reports on specific applications of our method have been given elsewhere.[42–44]

II. PROPERTIES OF THE HAMILTONIAN

The general problem we are concerned with is that of the motion of one electron and two (bare) nuclei under the influence of their mutual Coulomb interactions and of an external, uniform (static) magnetic field. The full quantum-mechanical solution of this three-body problem is hardly feasible at present. Due to the nonzero net charge of the system composed of one electron and two positively charged nuclei, the total linear momentum of this system is no longer conserved in the presence of an external magnetic field, and the center-of-mass motion can no longer be separated in the Hamiltonian.[15,45–48] This feature increases the complexity of the three-body problem far beyond that already encountered in the field-free case. Consequently, previous attempts[21–27,29–34,36–40] to calculate properties of magnetically dressed one-electron molecular ions have been based throughout on the strict Born-Oppenheimer approximation in which the nuclear coordinates are kept fixed, thereby reducing the three-body problem to a quantum-mechanical one-electron problem involving the nuclear coordinates as parameters. In the present paper, we also adhere to the Born-Oppenheimer approximation.

In the nonrelativistic approximation, the Hamiltonian describing the motion of an electron (with position vector $\mathbf{r}$) exposed to the Coulomb fields of two nuclei (with charge numbers Z_1, Z_2, and position vectors $\mathbf{R}_1, \mathbf{R}_2$, respectively) and to a uniform, static magnetic field $\mathbf{B}$ is given by

$$H=\frac{1}{2}\left[-i\nabla+\frac{1}{c}\mathbf{A}(\mathbf{r})\right]^2-\left[\frac{Z_1}{|\mathbf{r}-\mathbf{R}_1|}+\frac{Z_2}{|\mathbf{r}-\mathbf{R}_2|}\right] \tag{1}$$

(we use atomic units unless stated otherwise: $e=m_e=\hbar=1$; in these units, we have $c=137.04$ and $B_0=c$). The position vectors $\mathbf{r},\mathbf{R}_1,\mathbf{R}_2$ refer to an arbitrary, common origin. In writing Eq. (1), we have disregarded the coupling of the magnetic field to the spin of the electron, which gives an additional contribution to the energy of $+B/2c$ ($-B/2c$) if the spin is aligned parallel (antiparallel) to the field direction. The vector potential $\mathbf{A}(\mathbf{r})$ satisfying $\mathbf{B}=\nabla\times\mathbf{A}(\mathbf{r})$ is taken here in the "symmetric" gauge,

$$\mathbf{A}(\mathbf{r})=\tfrac{1}{2}(\mathbf{B}\times\mathbf{r}) . \tag{2}$$

Thereby, the Hamiltonian H acquires the explicit form

$$H=-\tfrac{1}{2}\nabla^2-\left[\frac{Z_1}{|\mathbf{r}-\mathbf{R}_1|}+\frac{Z_2}{|\mathbf{r}-\mathbf{R}_2|}\right]+\frac{B}{2c}(\hat{\mathbf{B}}\cdot l)+\frac{B^2}{8c^2}[r^2-(\hat{\mathbf{B}}\cdot\mathbf{r})^2] , \tag{3}$$

where $l=-i(\mathbf{r}\times\nabla)$ is the electronic orbital angular momentum about the chosen coordinate origin, and $\hat{\mathbf{B}}\equiv\mathbf{B}/B$.

It is appropriate to consider at this point the consequences of a shift of the "center of gauge," i.e., the consequences of replacing the electronic coordinate vector $\mathbf{r}$ in the vector potential $\mathbf{A}$ of Eq. (2) by $\mathbf{r}-\mathbf{s}$, where $\mathbf{s}$ is a constant vector. This replacement induces a gauge transformation

$$\mathbf{A}(\mathbf{r})\rightarrow\mathbf{A}(\mathbf{r})-\tfrac{1}{2}(\mathbf{B}\times\mathbf{s})\equiv\mathbf{A}(\mathbf{r})+\nabla f(\mathbf{r}) , \tag{4}$$

$$f(\mathbf{r})=-\tfrac{1}{2}(\mathbf{B}\times\mathbf{s})\cdot\mathbf{r} , \tag{5}$$

under which the Hamiltonian H transforms according to

$$H\rightarrow\exp\left[-\frac{i}{c}f\right]H\exp\left[\frac{i}{c}f\right]=-\tfrac{1}{2}\nabla^2-\left[\frac{Z_1}{|\mathbf{r}-\mathbf{R}_1|}+\frac{Z_2}{|\mathbf{r}-\mathbf{R}_2|}\right]+\frac{B}{2c}(\hat{\mathbf{B}}\cdot l_s)-\frac{B^2}{8c^2}\{(\mathbf{r}-\mathbf{s})^2-[\hat{\mathbf{B}}\cdot(\mathbf{r}-\mathbf{s})]^2\} , \tag{6}$$

where $l_s=l-\mathbf{s}\times\mathbf{p}$. The (exact) wave functions $\psi(\mathbf{r})$ associated with the Hamiltonian H transform under the gauge transformation (4) according to

$$\psi(\mathbf{r})\rightarrow\exp\left[-\frac{i}{c}f\right]\psi(\mathbf{r})=\exp\left[\frac{i}{2c}(\mathbf{B}\times\mathbf{s})\cdot\mathbf{r}\right]\psi(\mathbf{r}) . \tag{7}$$

The transformation properties of the Hamiltonian and the wave functions under a shift of the center of gauge are of relevance to the discussion of the separation behavior of magnetically dressed molecular orbitals at large internuclear distances, i.e., their dissociation into the orbitals of the separated atoms (cf. Sec. V). It should be mentioned that the observable quantities derived from a (necessarily approximate) numerical diagonalization of the Hamiltonian (8) in general depend on the choice for the center of gauge. However, this dependence is expected to be weak for "numerically converged" results.

In order to specify completely the Hamiltonian used in the present calculations, we choose the midpoint of the internuclear line as coordinate origin *and* center of gauge, and introduce coordinates x,y,z such that the z axis coincides with the internuclear axis and that the y axis is perpendicular to the field vector $\mathbf{B}$, i.e., $B_x = B\sin\theta$, $B_y = 0$, $B_z = B\cos\theta$, where θ is the angle between field vector and z axis. The Hamiltonian (3) then reads

$$H = -\tfrac{1}{2}\nabla^2 - \left(\frac{Z_1}{r_1}+\frac{Z_2}{r_2}\right) + \frac{B}{2c}(\cos\theta\, l_z + \sin\theta\, l_x) + \frac{B^2}{8c^2}[(x^2+y^2) - \sin^2\theta\,(x^2-z^2) - \sin 2\theta\, xz] \ , \tag{8}$$

where $r_{1,2} = |\mathbf{r}\pm\mathbf{R}/2|$ are the distances of the electron from the centers labeled 1 and 2, respectively, and $\mathbf{R} = \mathbf{R}_2 - \mathbf{R}_1$ is the internuclear vector.

In specific cases, the Hamiltonian (8) possesses certain symmetry properties which may be exploited in its diagonalization by restricting the basis set to functions of well-defined symmetry character. In charge symmetric systems, the parity operator P evidently commutes with the Hamiltonian (8),

$$[H,P] = 0 \quad \text{if } Z_1 = Z_2, \ \theta \text{ arbitrary} \ . \tag{9}$$

(Note that this symmetry is destroyed when the center of gauge is shifted away from the midpoint of the internuclear line.) When the magnetic field is parallel to the internuclear axis, the angular momentum component l_z is a good quantum number,

$$[H,l_z] = 0 \quad \text{if } \theta = 0, \ \ Z_1, Z_2 \text{ arbitrary} \ . \tag{10}$$

If P and l_z are good quantum numbers, the z-parity operation P_z which reverses the sign of the z coordinate is evidently also a good quantum number and can be used instead of P to label the eigenfunctions of H. When the field is perpendicular to the internuclear axis, H commutes with the operator P_x which reverses the sign of the x coordinate:

$$[H,P_x] = 0 \quad \text{if } \theta = 90°, \ \ Z_1, Z_2 \text{ arbitrary} \ . \tag{11}$$

In a representation in which the angular momentum component l_z (quantum number m) is diagonal, the selection rules for the field-dependent terms in the Hamiltonian (8) are $\Delta m = \pm 1$ for the terms proportional to $\sin\theta\, l_x$ and $\sin 2\theta\, xz$, and $\Delta m = 0, \pm 2$ for the term proportional to $\sin^2\theta\, x^2$ (the remaining terms are diagonal in m).

For arbitrary Z_1, Z_2, and $0 \le \theta \le \pi/2$, the Hamiltonian (8) can be easily shown to obey the relation

$$H(\pi/2+\theta) = P_x H(\pi/2-\theta) P_x^{-1} \ . \tag{12a}$$

Since the P_x operation is equivalent to a change from a right-handed to a left-handed coordinate system, the eigenvalues ε of H must be invariant under this operation,

$$\varepsilon(\pi/2+\theta) = \varepsilon(\pi/2-\theta) \ , \tag{12b}$$

and the wave function $\psi(\pi/2+\theta)$ is related to $\psi(\pi/2-\theta)$ through

$$\psi(\pi/2+\theta) = P_x \psi(\pi/2-\theta) \ . \tag{12c}$$

To obtain the energies and wave functions in the full range $0 \le \theta \le \pi$, we may therefore restrict the diagonalization of H to the range $0 \le \theta \le \pi/2$.

We conclude the discussion of the properties of the Hamiltonian by considering the scaling behavior of its eigenvalues and the associated wave functions. By subjecting the electronic coordinates $\mathbf{r}$ in the Schrödinger equation $H\psi = \varepsilon\psi$ to the scale transformation $\mathbf{r} \to \mathbf{r}/Z_1$, it is easily shown that for arbitrary values of R,θ,B,Z_1, and of the "asymmetry" Z_2/Z_1, the scaling relations

$$\varepsilon(R,\theta;B;Z_1,Z_2/Z_1) = Z_1^2\,\varepsilon(Z_1 R,\theta;B/Z_1^2;Z_1=1,Z_2/Z_1) \tag{13}$$

and

$$\psi(\mathbf{r};R,\theta;B;Z_1,Z_2/Z_1) = Z_1^{3/2}\,\psi(Z_1\mathbf{r};Z_1 R,\theta;B/Z_1^2;Z_1=1,Z_2/Z_1) \tag{14}$$

hold.

III. DIAGONALIZATION OF THE HAMILTONIAN

The Schrödinger equation $H\psi = \varepsilon\psi$ with the Hamiltonian (8) is separable only in the limiting case $B = 0$, i.e., for the pure two-center Coulomb problem (which is known to be separable in prolate spheroidal coordinates). When attempting to solve the nonseparable problem posed for $B > 0$ by diagonalizing the Hamiltonian in a fixed basis, the selection of the basis functions will be mainly guided by the desire to construct functions which allow the problem to be adequately solved in as broad a B range as possible. If one excludes the possibility that the full range $0 < B < \infty$ can be covered simultaneously with one and the same type of basic functions, it is advisable to look for functions that are specifically adapted either to the low-B or to the high-B regime. In the latter regime, where the magnetic interaction prevails over the Coulomb interaction, appropriate basis functions must be required to adequately represent the limiting case of pure Landau orbitals. In the low-B regime, the choice of the basis functions is determined by the dominance of the two-center Coulomb potential.

The Hylleraas basis functions[41] which are used in the present work to calculate magnetically dressed one-electron molecular orbitals are particularly adapted to the low-B regime. Their definition in terms of prolate spheroidal coordinates allows the efficient diagonalization

of the pure two-center Coulomb problem as well as of more general (nonseparable) two-center problems involving screened two-center potentials.[49] In fact, the motivation to use the Hylleraas basis in the calculation of magnetically dressed molecular orbitals arose[42] from the possibility of using, in the special case $\theta=0$, a trivially modified version of a computer code devised for the diagonalization of screened two-center problems.

A. Properties of the Hylleraas basis

The (nonorthogonal) Hylleraas functions ψ_{nl}^{m} are defined in terms of prolate spheroidal coordinates $\xi=(r_1+r_2)/R$, $\eta=(r_1-r_2)/R$, $\phi=$azimuthal angle about the z axis, as

$$\psi_{nl}^{m}(\xi,\eta,\phi)=(2\pi)^{-1/2}\exp\left[-\frac{\xi-1}{2a}\right](\xi^2-1)^{m/2} \times L_n^m\left[\frac{\xi-1}{a}\right]P_l^m(\eta)\exp(im\phi) \tag{15a}$$

for $m\geq 0$ and

$$\psi_{nl}^{m}(\xi,\eta,\phi)=(-1)^{|m|}\psi_{nl}^{|m|\,*}(\xi,\eta,\phi) \tag{15b}$$

for $m<0$ ($n=0,1,\ldots$; $l=|m|,|m|+1,\ldots$). The functions L_n^m and P_l^m are generalized Laguerre polynomials and associated Legendre functions, respectively, and the quantity a is a dimensionless parameter which is assumed to be independent of the labels n, l, and m. The functions ψ_{nl}^{m} are eigenfunctions of the angular momentum component l_z (with eigenvalue m) and of the parity operator P [with eigenvalue $(-1)^l$]. Eigenfunctions of the reflection operator P_x may be constructed from the functions ψ_{nl}^{m} by defining, for $m>0$,

$$\psi_{nl}^{m(\pm)}=\frac{1}{\sqrt{2}}(1\pm P_x)\psi_{nl}^{m}\equiv\frac{1}{\sqrt{2}}(\psi_{nl}^{m}\pm\psi_{nl}^{-m})\ ; \tag{16}$$

the functions $\psi_{nl}^{m(+)}$, as well as the functions $\psi_{nl}^{m=0}$, are even under P_x, while the functions $\psi_{nl}^{m(-)}$ are odd under this operation. This behavior is exploited in the diagonalization of the Hamiltonian (8) in the case $\theta=90°$, in which H commutes with P_x [cf. Eq. (11)].

We note here that the elements of the overlap matrix $\underline{N}$,

$$N_{nl,n'l'}^{m,m'}=\langle\,\psi_{nl}^{m}\,|\,\psi_{n'l'}^{m'}\,\rangle\ , \tag{17}$$

can be evaluated in closed form. Details of the evaluation are given in the Appendix.

The convergence properties of the Hylleraas basis are decisively influenced by the choice of the value of the parameter a. In the case of the pure two-center Coulomb problem, the value of a can be fixed by requiring the exponential factor $\exp[-(\xi-1)/2a]$ to match asymptotically, i.e, for $r_1,r_2\rightarrow\infty$, the exponentially decaying tail of the wave function of a specific united-atom orbital with principal quantum number n^{UA} (note that for arbitrary, finite internuclear distance R, an electron at infinity "sees" a united-atom nucleus with charge number Z_1+Z_2). This criterion leads to the prescription

$$a=\frac{n^{\mathrm{UA}}}{(Z_1+Z_2)R}\ , \tag{18}$$

which indeed turns out[49] to be an adequate choice for a at not-too-large R values (a somewhat modified prescription to calculate a is appropriate in cases where R is so large that the separated-atom character of the orbitals dominates).

No simple prescription for the calculation of a can be given if the Hylleraas basis is used in the solution of the two-center Coulomb problem with superimposed strong magnetic field. The main effect of the field is to elongate the electronic wave function in the field direction and to constrict it in the direction perpendicular to the field. The behavior of the tail of the wave function in the latter direction changes from exponential to Gaussian when the field strength increases. Such a behavior can be hardly simulated by a single exponential,[50] so that, in order to achieve convergence of the Hylleraas expansion, a large number of Laguerre polynomials and Legendre functions will have to be included, in general. Any optimum value for a thus reflects the complicated interplay of exponential and nonexponential parts of the basis, and an *a priori* determination of this value seems prohibitively complicated. In our calculations, we employ the prescription (18) but allow the quantum number n^{UA} to become a field-dependent, effective parameter $n_{\mathrm{eff}}(B)$ whose value can be roughly optimized by performing sequences of calculations with different values of n_{eff} and looking for the minimum energy of particular states.

One can, of course, increase the flexibility of the Hylleraas basis by allowing the parameter a to be dependent on the labels n, l, and m. It appears, however, a difficult task to develop an efficient strategy for determining the *optimal* dependence of a on n, l, and m. We therefore defer the development and application of such a strategy to future investigations.

B. Solution of the generalized eigenvalue problem for the Hamiltonian matrix

The Schrödinger equation $H\psi=\varepsilon\psi$ with the Hamiltonian (8) is solved by expanding the wave function ψ in terms of the Hylleraas functions ψ_{nl}^{m} as

$$\psi=\sum_{n,l,m}c_{nl}^{m}\psi_{nl}^{m}\ , \tag{19}$$

where $n=0,1,\ldots,n_{\max}$; $l=|m|,|m|+1,\ldots,l_{\max}$; $m=0,\pm1,\ldots,\pm m_{\max}$. This leads to the generalized eigenvalue problem

$$\underline{H}\mathbf{c}=\varepsilon\underline{N}\mathbf{c} \tag{20}$$

for the (real and symmetric) Hamiltonian matrix $\underline{H}$. The overlap matrix $\underline{N}$ is real, symmetric, and positive definite, and the vector $\mathbf{c}$ comprises the expansion coefficients c_{nl}^{m}.

A major advantage of the Hylleraas basis is that it allows a completely analytic evaluation of the elements of $\underline{H}$ and $\underline{N}$. All matrix elements can be expressed in terms of two types of basic integrals which can be easily evaluated in closed form by means of recurrence relations. Details of this procedure are given in the Appendix.

For the numerical solution of the eigenvalue problem (20), we use standard methods. We first calculate the full set of eigenvalues and eigenvectors of the overlap matrix $\underline{N}$, so that N may be written as

$$\underline{N}=\underline{O}_N\underline{N}_D\underline{O}_N^T , \tag{21}$$

where $\underline{N}_D$ is the diagonal matrix built up from the eigenvalues of $\underline{N}$, and $\underline{O}_N$ is the (orthogonal) matrix composed of the associated eigenvectors ($\underline{O}_N^T$ denotes the transpose of $\underline{O}_N$). The diagonalization of $\underline{N}$ is substantially simplified by the fact that this matrix is diagonal in the label m and that its elements are independent of the sign of m [cf. Eq. (A15)]. For the construction of the matrix $\underline{O}_N$, it is therefore sufficient to diagonalize separately the overlap matrices in the m subspaces with $m=0,1,\ldots,m_{\max}$. Having obtained $\underline{N}_D$ and $\underline{O}_N$, the problem (20) can be transformed into the standard eigenvalue problem

$$\underline{\tilde{H}}\tilde{\mathbf{c}}=\varepsilon\tilde{\mathbf{c}} \tag{22}$$

for the matrix $\underline{\tilde{H}}$ given by

$$\underline{\tilde{H}}=\underline{N}_D^{-1/2}\underline{O}_N^T\underline{H}\,\underline{O}_N\underline{N}_D^{-1/2} . \tag{23}$$

The vector $\tilde{\mathbf{c}}$ is related to $\mathbf{c}$ by

$$\tilde{\mathbf{c}}=\underline{N}_D^{1/2}\underline{O}_N^T\mathbf{c} . \tag{24}$$

We solve the problem (21) for the full eigenvalue spectrum and for selected eigenvectors by using standard diagonalization routines. In the actual calculations, limitations with respect to computer storage restrict the largest total dimension of the basis space to be less than about 500. A substantial improvement of the efficiency of the procedure used to solve the problem (20) is presumably possible. One possibility, which will be the subject of future investigations, is the exploitation of the band structure of the Hamiltonian matrix as determined by the selection rules (A48). We note that we have not found any indications of numerical instabilities in our calculations. However, a careful investigation of possible instabilities seems necessary if the dimension of the basis space is increased far beyond the present maximum value.

IV. GENERAL PROPERTIES OF MAGNETICALLY DRESSED ONE-ELECTRON MOLECULAR ORBITALS: THE CASE $\theta=0$

A separate discussion of the case $\theta=0$ is advisable for several reasons. (i) The Hamiltonian (8) contains four parameters [$Z_2/Z_1,R,B,\theta$; note the scaling relations (13) and (14)] whose values can be independently varied within their physical boundaries. Therefore, in a first application of our method, it is appropriate to keep the values of one or two of these parameters fixed in order not to get lost in the full complexity of the problem. (ii) The case $\theta=0$ is distinguished by the fact that the angular momentum projection m is a good quantum number and that, accordingly, at a given level of accuracy, the effort spent to diagonalize the Hamiltonian is drastically smaller than in the case $\theta\neq 0$. Alternatively, for a given maximum basis size, the accuracy of the $\theta=0$ results can be pushed to a much higher degree. (iii) Previous calculations dealing with magnetically dressed molecular orbitals have considered almost exclusively the H_2^+ system at $\theta=0$. To establish our method, a systematic comparison of our results for this specific case with those of the previous investigations seems indicated.

The calculations for the case $\theta=0$ can be restricted to non-negative m values, since the Hamiltonian matrix for fixed m is, after subtraction of the diagonal Zeeman term $(B/2c)m$, independent of the sign of m. The wave functions ψ_m for $m<0$ are expressed in terms of those for $m>0$ as $\psi_m=(-)^{|m|}\psi^*_{|m|}$ [cf. Eq. (15b)]. The magnetically dressed molecular orbitals are labeled $1\sigma,\ 2\sigma,\ldots,1\pi(m=\pm1),2\pi(m=\pm1),\ldots,1\delta(m=\pm2),2\delta(m=\pm2),\ldots,$ with an additional subscript g or u (corresponding to "gerade" and "ungerade," respectively) to indicate the parity of the orbital in the charge symmetric case $Z_1=Z_2$ [note that some authors[32,34] use the labels g and u to denote the quantum number associated with the z-parity operation $z\rightarrow -z$; this quantum number differs from the quantum number of the full parity operation, which *we* label g or u, by a factor $(-)^m$]. In the limiting case $B=0$, we use the usual united-atom notation $1s\sigma,2p\sigma,\ldots,2p\pi,\ldots$ to label the molecular orbitals.

In the following, we present and discuss our results for the magnetically dressed H_2^+ and $(H\text{-}He)^{2+}$ systems. In particular, we consider the effect of the magnetic field on the electronic orbitals energies, on equilibrium internuclear distances, and on the electronic wave functions.

A. Orbital energies and molecular-orbital correlation diagrams

At fixed field strength B and angle θ, the influence of a strong magnetic field on molecular orbitals can be visualized by drawing correlation diagrams in which electronic orbital energies are plotted as a function of internuclear distance R.

Figure 1 shows the correlation diagram for the magnetically dressed H_2^+ system at $B=B_0$ and $\theta=0$ (including the lowest orbitals of given symmetry up to $|m|=2$) in comparison with the diagram for the field-free case. In order to emphasize the overall behavior of the energy curves, we have suppressed the Zeeman splitting of the curves for nonzero m values, i.e., each of the drawn solid curves gives the centroid energy of Zeeman doublets corresponding to $m=\pm|m|$. Three obvious effects of the magnetic field can be identified in Fig. 1. (i) The field causes an increase of the orbital energies, which becomes larger with increasing value of $|m|$. This feature reflects the decrease of the Coulomb interaction and the linear rise of the purely magnetic (Landau) energy with increasing $|m|$. (ii) The united-atom ($R=0$) degeneracy of levels with different $|m|$ values is removed (compare, e.g., the behavior of the $1\sigma_u$ and $1\pi_u$ curves to that of the $2p\sigma$ and $2p\pi$ curves). (iii) At large internuclear distances, the field tends to reduce the g-u splitting of energy curves which are degenerate in the separated-atom ($R=\infty$) limit. This effect is related to the field-induced increase of the electronic *binding* ener-

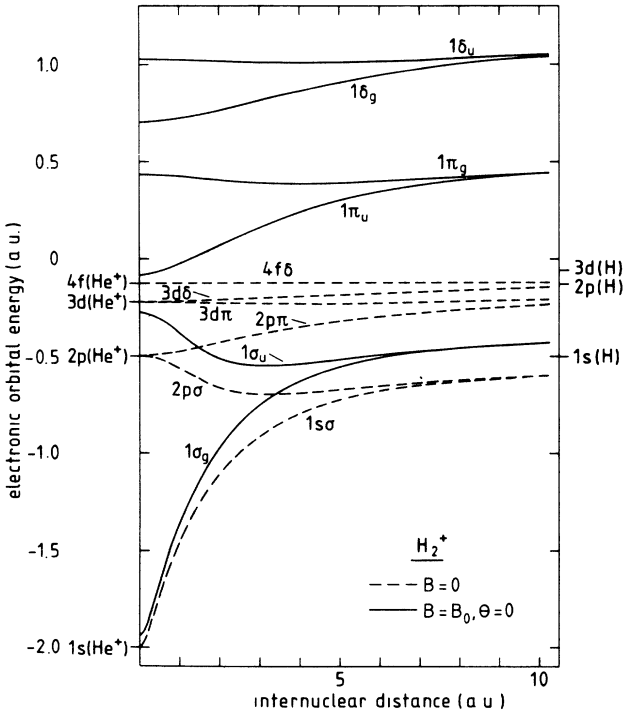

FIG. 1. Orbital energy correlation diagram for the H_2^+ system. Dashed curves: $B=0$; solid curves: $B=B_0$, $\theta=0$. The Zeeman splitting of the energy curves for $B=B_0$, $|m|>0$ has been suppressed. The united-atom and separated-atom energies correspond to $B=0$, and the usual united-atom designation is used to label the $B=0$ energy curves.

gy, which is associated, at large internuclear distances, with an increased localization of the wave function in the vicinity of either nuclear center (cf. Secs. IV C and V D).

Numerical values corresponding to the dressed energy curves of Fig. 1 are given in Table I. The quoted numbers for $R>0$ have been calculated by taking throughout a value of 1.0 for the parameter n_{eff} and including up to 231 functions in the Hylleraas basis [the largest dimension of the basis space corresponds to $n_{\max}=20$, $l_{\max}=|m|+20$; note the parity selection rule (A48d) for the label l]. The numbers given for $R=0$ have been obtained by extrapolating energies calculated for very small R, assuming a quadratic R dependence of the energies in this range (note that our diagonalization procedure breaks down at $R=0$). Within the given accuracy, the results of Table I are converged results in the sense that they remain unchanged under a further extension of the basis space as well as under a variation of the value of n_{eff} within rather broad limits. We have not attempted to find, separately for each orbital and each R value, the minimum basis set that allows the energies to be calculated to a prescribed accuracy. To achieve the accuracy of the numbers given in Table I, the maximum basis size of 231 is required only for the calculation of the π and δ orbitals at the largest R values. In the small-R range, basis sets with dimension less than 100 are sufficient throughout.

The main use of molecular-orbital correlation diagrams, both in the field-free case and in the magnetically dressed case, is in the investigation of electronic transitions in quasimolecules formed transiently in ion-atom collisions. Diagrams appropriate to the discussion of this situation have to display the total electronic orbital energy on a scale which places the ionization threshold at zero energy. Equivalently, one may plot the electronic *binding* energy ε_b, which for the magnetically dressed case is given by

$$\varepsilon_b=\varepsilon_{\text{th}}-\varepsilon\ , \tag{25}$$

where ε is the total electronic orbital energy [including the contribution $(B/2c)m$ of the linear Zeeman term] on the scale defined by the Hamiltonian (8). On this scale, the threshold energy ε_{th} for arbitrary m values is given by the lowest energy which an (otherwise free) electron can have in a magnetic field, i.e., by the energy of the lowest Landau state, $\varepsilon_{\text{th}}=B/2c\equiv B/2B_0$.

In Fig. 2, we show the binding energy correlation diagram for the magnetically dressed H_2^+ system at $B=B_0$ and $\theta=0$, in comparison with the field-free diagram. The dressed energy curves for $|m|>0$ all refer to the case $m=-|m|$. In comparison with the latter curves, the curves for $m=+|m|$ are, on the scale of Fig. 2, shifted upwards by the Zeeman splitting (which, for $B=B_0$, amounts to $|m|$ a.u.). Hence at $B=B_0$ all orbitals with $m=+|m|>0$ are formally unbound [except for the $1\pi_u(m=+1)$ orbital which crosses the ionization threshold at $R\simeq 1.25$ a.u.].

A noteworthy feature of the correlation diagram of Fig. 2 is the appearance of real crossings (at $R>0$) of energy curves whose field-free counterparts merge at $R=0$, viz., the $1\sigma_u$-$1\pi_u$ crossing at $R\simeq 1.6$ a.u. and the

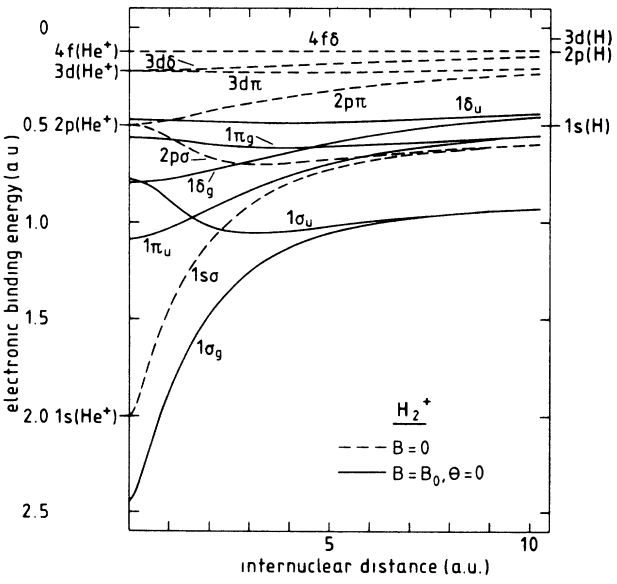

FIG. 2. Binding-energy correlation diagram corresponding to the orbital energy correlation diagram of Fig. 1. The energy curves for $B=B_0$, $|m|>0$ include the Zeeman splitting and all refer to $m=-|m|$.

$1\pi_g$-$1\delta_g$ crossing at $R \simeq 4.5$ a.u. When assessing the influence of these crossings on electronic excitation processes, one has to keep in mind, of course, that the real crossings (of one and the same parity) at $\theta=0$ turn into avoided crossings when $\theta \neq 0$, and progressively lose their identity with increasing θ. We return to a discussion of this point in Sec. V.

The orbital-energy correlation diagram and the binding-energy correlation diagram for the asymmetric $(\text{H-He})^{2+}$ system at $B=B_0$ and $\theta=0$ are shown in Figs. 3 and 4, respectively, in comparison with the field-free diagram. The Zeeman splitting has been suppressed in Fig. 3, and the dressed energy curves of Fig. 4 all refer to $m=-|m|$. Numerical values corresponding to the dressed curves of Fig. 3 are presented in Table II. These values have been calculated by using up to 441 basis functions (the latter number corresponds to $n_{\max}=20$, $l_{\max}=|m|+20$; note the absence of a parity selection rule for asymmetric systems). As in the H_2^+ case, the maximum dimension of the basis space is required only for the largest R values. With regard to the qualitative influence of the magnetic field, the remarks made in conjunction with the H_2^+ system also apply to the $(\text{H-He})^{2+}$ case.

TABLE I. Energies (in a.u.) of the lowest orbitals of the magnetically dressed H_2^+ system at $B=B_0$ and $\theta=0$, for different values of the internuclear distance R (in a.u.). The contribution of the linear Zeeman term to the energy of the $m \neq 0$ orbitals has been omitted. For accuracy of the numbers, see text.

R	$\varepsilon_{1\sigma_g}$	$\varepsilon_{1\sigma_u}$	$\varepsilon_{1\pi_u}$	$\varepsilon_{1\pi_g}$	$\varepsilon_{1\delta_g}$	$\varepsilon_{1\delta_u}$
0	−1.9412	−0.2756	−0.0832	0.4375	0.7059	1.0290
0.25	−1.834 48	−0.282 97	−0.078 77	0.436 81	0.707 02	1.028 79
0.5	−1.661 51	−0.304 68	−0.066 52	0.434 68	0.710 57	1.028 23
0.75	−1.498 42	−0.338 72	−0.048 61	0.431 29	0.716 28	1.027 25
1.0	−1.357 23	−0.380 24	−0.027 01	0.426 89	0.723 85	1.025 95
1.25	−1.236 94	−0.422 85	−0.003 27	0.421 78	0.732 94	1.024 39
1.5	−1.134 37	−0.461 23	0.021 53	0.416 30	0.743 25	1.022 66
1.75	−1.046 42	−0.492 60	0.046 63	0.410 76	0.754 48	1.020 84
2.0	−0.970 54	−0.516 33	0.071 54	0.405 45	0.766 38	1.019 01
2.25	−0.904 73	−0.533 04	0.095 92	0.400 60	0.778 74	1.017 24
2.5	−0.847 42	−0.543 84	0.119 54	0.396 37	0.791 38	1.015 59
2.75	−0.797 34	−0.549 94	0.142 29	0.392 85	0.804 13	1.014 13
3.0	−0.753 51	−0.552 39	0.164 07	0.390 09	0.816 89	1.012 90
3.25	−0.715 11	−0.552 10	0.184 83	0.388 09	0.829 56	1.011 93
3.5	−0.681 45	−0.549 78	0.204 57	0.386 82	0.842 05	1.011 23
3.75	−0.651 95	−0.546 01	0.223 28	0.386 23	0.854 30	1.010 81
4.0	−0.626 11	−0.541 22	0.240 96	0.386 26	0.866 26	1.010 67
4.25	−0.603 48	−0.535 75	0.257 64	0.386 83	0.877 91	1.010 81
4.5	−0.583 66	−0.529 86	0.273 33	0.387 89	0.889 20	1.011 22
4.75	−0.566 29	−0.523 74	0.288 08	0.389 35	0.900 11	1.011 87
5.0	−0.551 05	−0.517 54	0.301 90	0.391 17	0.910 63	1.012 75
5.25	−0.537 64	−0.511 36	0.314 82	0.393 27	0.920 75	1.013 83
5.5	−0.525 82	−0.505 28	0.326 89	0.395 61	0.930 47	1.015 10
5.75	−0.515 35	−0.499 36	0.338 14	0.398 14	0.939 77	1.016 54
6.0	−0.506 05	−0.493 64	0.348 59	0.400 81	0.948 66	1.018 11
6.25	−0.497 74	−0.488 14	0.358 30	0.403 59	0.957 13	1.019 81
6.5	−0.490 27	−0.482 86	0.367 29	0.406 44	0.965 20	1.021 62
6.75	−0.483 53	−0.477 83	0.375 61	0.409 34	0.972 86	1.023 50
7.0	−0.477 42	−0.473 04	0.383 30	0.412 26	0.980 12	1.025 46
7.25	−0.471 84	−0.468 49	0.390 39	0.415 18	0.986 99	1.027 48
7.5	−0.466 73	−0.464 16	0.396 94	0.418 09	0.993 49	1.029 53
7.75	−0.462 02	−0.460 06	0.402 98	0.420 97	0.999 61	1.031 61
8.0	−0.457 66	−0.456 17	0.408 55	0.423 81	1.005 38	1.033 70
8.25	−0.453 62	−0.452 49	0.413 69	0.426 60	1.010 80	1.035 81
8.5	−0.449 85	−0.448 99	0.418 43	0.429 32	1.015 89	1.037 91
8.75	−0.446 33	−0.445 67	0.422 82	0.431 98	1.020 66	1.040 00
9.0	−0.443 02	−0.442 53	0.426 89	0.434 58	1.025 14	1.042 07
9.25	−0.439 91	−0.439 54	0.430 66	0.437 10	1.029 33	1.044 12
9.5	−0.436 98	−0.436 70	0.434 16	0.439 54	1.033 26	1.046 14
9.75	−0.434 21	−0.434 00	0.437 42	0.441 92	1.036 93	1.048 13
10.0	−0.431 59	−0.431 43	0.440 47	0.444 22	1.040 37	1.050 08

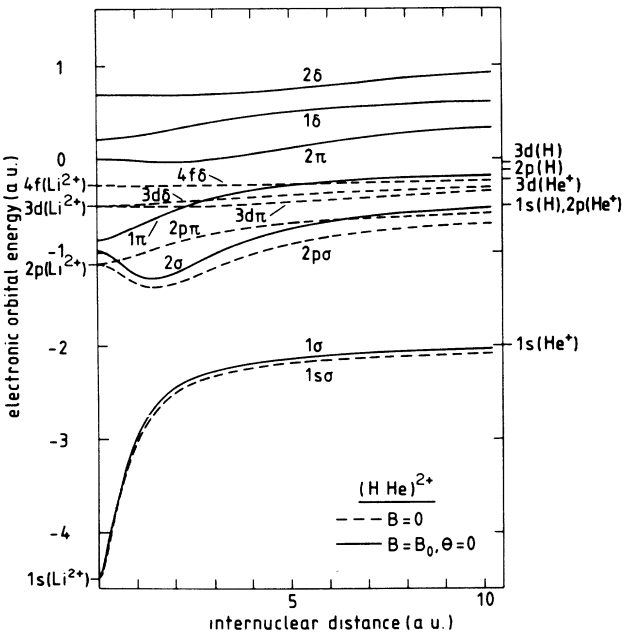

FIG. 3. Same as Fig. 1, for the $(H\text{-}He)^{2+}$ system.

B. Equilibrium internuclear distances and total binding energies

For a detailed comparison of our method to previous work of other authors, we consider now total energies (potential curves) of the magnetically dressed H_2^+ system at $\theta=0$, as well as equilibrium internuclear distances and binding energies.

The total energies $E(R)=\varepsilon(R)+1/R$ of the $1\sigma_g$ state of the dressed H_2^+ system are shown in Fig. 5 for different values of the field strength. The curves demonstrate the well-known[22] decrease of the equilibrium internuclear distance with increasing field strength, which is ascribed to the enhanced screening of the protons due to the enhanced electron density on the internuclear line between the protons (cf. Sec. IV C).

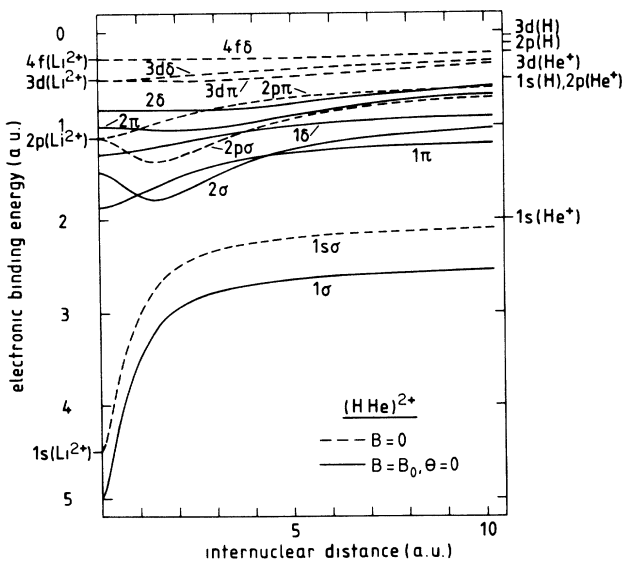

FIG. 4. Same as Fig. 2, for the $(H\text{-}He)^{2+}$ system.

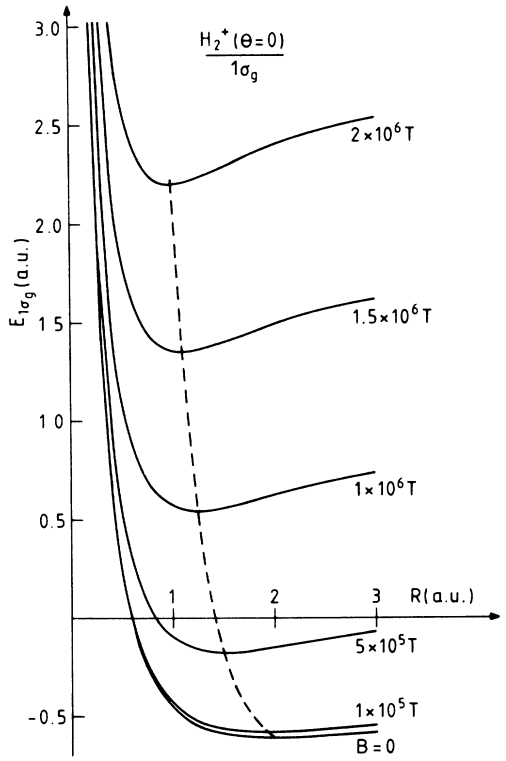

FIG. 5. Total energy of the magnetically dressed H_2^+ system in the electronic $1\sigma_g$ state at $\theta=0$, plotted as function of internuclear distance R for various values of the field strength B. The dashed curve connects the positions of the minima of the different potential curves.

The B dependence of the equilibrium internuclear dis-

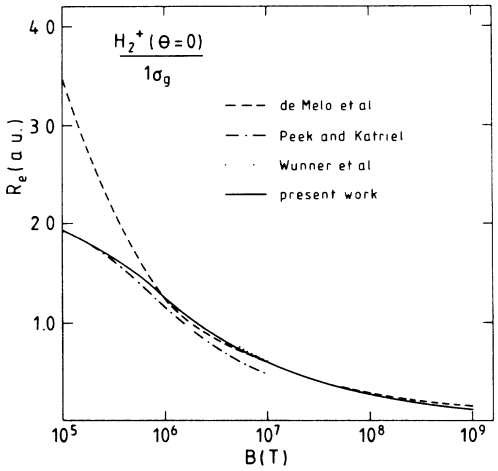

FIG. 6. Equilibrium internuclear distance R_e of the magnetically dressed H_2^+ system in the electronic $1\sigma_g$ state at $\theta=0$, plotted as function of field strength B. The results of the present work are compared to those of de Melo *et al.* (Ref. 22), Peek and Katriel (Ref. 29), and Wunner *et al.* (Ref. 34).

tance R_e for the dressed H_2^+ system in the $1\sigma_g$ state is shown in Fig. 6. Numerical values pertaining to our calculations are given in Table III. The results obtained by our method are in very good agreement with those of Peek and Katriel[29] in the limit of small field strength. This was to be expected since Peek and Katriel use the most general function, which is separable in prolate spheriodal coordinates (in these coordinates, the pure two-center Coulomb problem is separable), as a trial wave function in their variational calculations. The results obtained by Vincke and Baye[40] in the range 2.35×10^6 T $\leq B \leq 4.7\times10^7$ T agree with our results within the accuracy of Fig. 6. Beyond $B=5\times10^7$ T, our values for R_e begin to depart from those of de Melo *et al.*[22] and of Wunner *et al.*[34] The latter two calculations use trial wave functions which approach the lowest Landau orbital in the high-field limit and which are therefore superior to our wave functions in this limit.

The breakdown of our method in the high-field limit becomes more apparent in the total energies E_e at the equilibrium internuclear distance R_e and in the corresponding total binding energies $E_e^{(b)}=\varepsilon_{\rm th}-\varepsilon_e-1/R_e$. Numerical values for these quantities for different values of the field strength B are given in Table III. The total binding energies are compared in Fig. 7 to the results of de Melo *et al.*,[22] Peek and Katriel,[29] and Wunner *et al.*[34] While the agreement of our results with those of Peek and Katriel in the low-field limit is again very good, our

TABLE II. Energies (in a.u.) of the lowest orbitals of the magnetically dressed $(H\text{-}He)^{2+}$ system at $B=B_0$ and $\theta=0$, for different values of the internuclear distance R (in a.u.). The contribution of the linear Zeeman term to the energy of the $m\neq0$ orbitals has been omitted. For accuracy of the numbers, see text.

R	$\varepsilon_{1\sigma}$	$\varepsilon_{2\sigma}$	$\varepsilon_{1\pi}$	$\varepsilon_{2\pi}$	$\varepsilon_{1\delta}$	$\varepsilon_{2\delta}$
0	−4.4724	−0.9889	−0.8648	0.0000	0.2080	0.6881
0.25	−4.102 07	−1.011 89	−0.852 50	−0.001 40	0.210 45	0.687 85
0.5	−3.627 42	−1.076 17	−0.820 47	−0.005 21	0.217 73	0.687 11
0.75	−3.256 99	−1.160 79	−0.777 40	−0.010 82	0.229 10	0.686 00
1.0	−2.983 82	−1.233 66	−0.729 57	−0.017 27	0.243 70	0.684 68
1.25	−2.784 73	−1.274 41	−0.680 87	−0.023 56	0.260 68	0.683 35
1.5	−2.639 81	−1.281 15	−0.633 52	−0.028 72	0.279 28	0.682 20
1.75	−2.533 57	−1.261 55	−0.588 73	−0.032 00	0.298 85	0.681 43
2.0	−2.454 37	−1.224 97	−0.547 14	−0.032 89	0.318 86	0.681 23
2.25	−2.393 88	−1.179 16	−0.509 07	−0.031 11	0.338 88	0.681 74
2.5	−2.346 44	−1.129 40	−0.474 59	−0.026 61	0.358 60	0.683 07
2.75	−2.308 25	−1.079 10	−0.443 64	−0.019 51	0.377 76	0.685 30
3.0	−2.276 82	−1.030 19	−0.416 05	−0.010 03	0.396 15	0.688 48
3.25	−2.250 46	−0.983 80	−0.391 59	0.001 49	0.413 63	0.692 62
3.5	−2.228 01	−0.940 50	−0.369 97	0.014 71	0.430 12	0.697 71
3.75	−2.208 65	−0.900 53	−0.350 87	0.029 26	0.445 53	0.703 72
4.0	−2.191 76	−0.863 92	−0.333 99	0.044 76	0.459 86	0.710 57
4.25	−2.176 89	−0.830 60	−0.319 03	0.060 91	0.473 11	0.718 20
4.5	−2.163 70	−0.800 44	−0.305 73	0.077 41	0.485 31	0.726 50
4.75	−2.151 91	−0.773 22	−0.293 84	0.094 02	0.496 50	0.735 38
5.0	−2.141 32	−0.748 70	−0.283 17	0.110 54	0.506 75	0.744 73
5.25	−2.131 74	−0.726 64	−0.273 54	0.126 83	0.516 14	0.754 43
5.5	−2.123 04	−0.706 78	−0.264 81	0.142 76	0.524 74	0.764 38
5.75	−2.115 10	−0.688 86	−0.256 85	0.158 24	0.532 62	0.774 48
6.0	−2.107 82	−0.672 65	−0.249 58	0.173 20	0.539 86	0.784 65
6.25	−2.101 13	−0.657 93	−0.242 90	0.187 59	0.546 53	0.794 80
6.5	−2.094 96	−0.644 51	−0.236 74	0.201 37	0.552 68	0.804 87
6.75	−2.089 25	−0.632 22	−0.231 04	0.214 53	0.558 37	0.814 79
7.0	−2.083 94	−0.620 92	−0.225 76	0.227 05	0.563 64	0.824 52
7.25	−2.079 00	−0.610 49	−0.220 84	0.238 92	0.568 55	0.834 00
7.5	−2.074 40	−0.600 82	−0.216 26	0.250 14	0.573 13	0.843 21
7.75	−2.070 25	−0.591 79	−0.211 97	0.260 71	0.577 41	0.852 10
8.0	−2.066 05	−0.583 44	−0.207 95	0.270 64	0.581 41	0.860 65
8.25	−2.062 25	−0.575 60	−0.204 17	0.279 94	0.585 18	0.868 84
8.5	−2.058 68	−0.568 24	−0.200 62	0.288 59	0.588 71	0.876 62
8.75	−2.055 32	−0.561 33	−0.197 27	0.296 64	0.592 05	0.883 99
9.0	−2.052 14	−0.554 81	−0.194 11	0.304 05	0.595 20	0.890 91
9.25	−2.049 13	−0.548 66	−0.191 12	0.310 81	0.598 18	0.897 37
9.5	−2.046 28	−0.542 85	−0.188 28	0.316 91	0.601 00	0.903 34
9.75	−2.043 58	−0.537 34	−0.185 59	0.322 32	0.603 67	0.908 81
10.0	−2.041 02	−0.532 12	−0.183 04	0.327 06	0.606 21	0.913 80

TABLE III. Equilibrium internuclear distance R_e, total energy E_e, and total binding energy $E_e^{(b)}$ of the magnetically dressed H_2^+ system in the electronic $1\sigma_g$ state at $\theta=0$, for different values of the magnetic field strength B.

B (T)	R_e (a.u.)	E_e (a.u.)	$E_e^{(b)}$ (a.u.)
0	1.997	−0.602 635	0.602 635
10^5	1.924	−0.575 359	0.788 125
2×10^5	1.795	−0.505 980	0.931 513
5×10^5	1.503	−0.174 751	1.238 60
10^6	1.246	0.545 154	1.582 51
2×10^6	1.008	2.208 50	2.046 83
5×10^6	0.747	7.744 76	2.893 74
10^7	0.593	17.5214	3.7552
2×10^7	0.472	37.7019	4.8513
5×10^7	0.350	99.6574	6.7276
10^8	0.278	204.283	8.483
2×10^8	0.220	415.124	10.409
5×10^8	0.159	1051.46	12.40
7.5×10^8	0.138	1583.31	12.42
10^9	0.125	2115.91	11.76

calculated binding energies are slightly larger than those of de Melo *et al.* and of Wunner *et al.* (and also those of Vincke and Baye[40] in the range 10^6 T $\leq B \leq 5\times10^7$ T). Beyond $B=10^8$ T, our results become progressively smaller than those of the methods which are specifically adapted to the high-field limit.

Our results given in Table III and displayed in Fig. 6 have been obtained by employing a basis space with $n_{max}=20$, $l_{max}=20$ throughout. Within this space, we have optimized the value of the parameter n_{eff} by minimizing the total energy E_e with respect to it. In Fig. 8 we show the dependence of $\Delta E_e = E_e - E_e^{(min)}$ (where $E_e^{(min)}$ is the minimum equilibrium energy) on n_{eff} for different values of the field strength. It is seen that E_e is virtually independent on n_{eff} in a "window" that narrows with increasing field strength. This behavior corresponds to the field-induced increase of the binding energy which requires the wave function to decrease more rapidly at large distances (note that smaller n_{eff} values imply a larger decay constant in the exponential part of the Hylleraas functions).

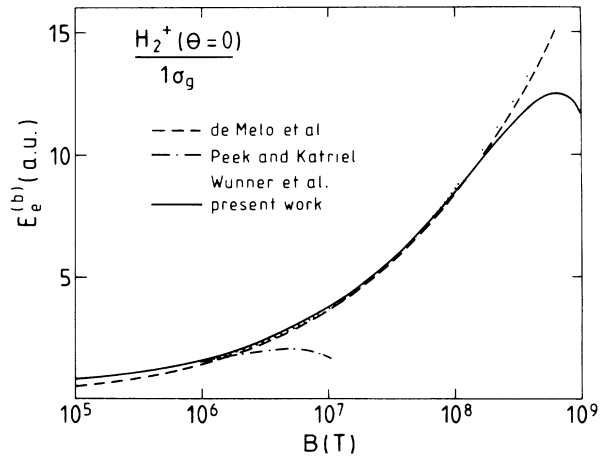

FIG. 7. Total binding energies $E_e^{(b)}$ corresponding to the equilibrium internuclear distances of the H_2^+ system shown in Fig. 6.

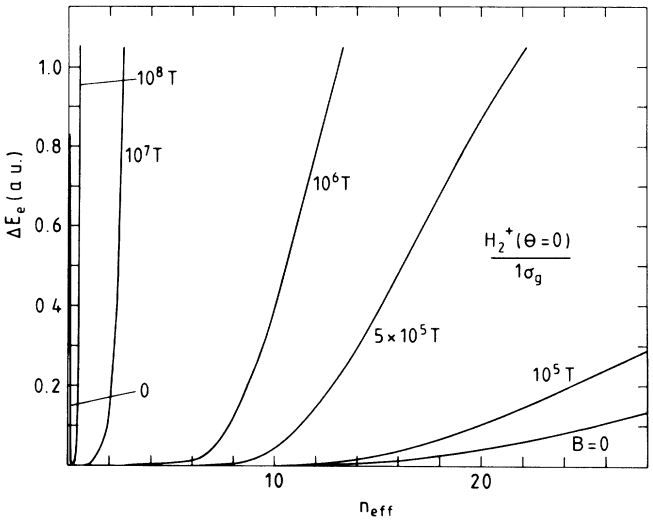

FIG. 8. Difference ΔE_e of total equilibrium energy and the corresponding minimum energy (obtained by optimizing the value of the parameter n_{eff}) for the magnetically dressed H_2^+ system at $\theta=0$, plotted as function of n_{eff} for various values of the field strength B. For $B>0$, only the right-hand branches of the curves are shown. The left-hand branches of these curves virtually coincide with the corresponding branch of the $B=0$ curve.

Using the same basis size as in the calculations on the $1\sigma_g$ state, as well as the optimized n_{eff} values obtained for this case, we have calculated total binding energies for the magnetically dressed H_2^+ system in the lowest states with $m=-1$, -2, -3, and -4 and *even* z parity. The field-induced decrease of the equilibrium internuclear distance and the gain in binding energy are expected to be in the even-z-parity states considerably more pronounced than in the odd states, since the field-induced accumulation of the electron density between the two protons will be larger in the even states. The equilibrium distances R_e and binding energies $E_e^{(b)}$ of the lowest states of even z parity have been calculated by Vincke and Baye[40] for field strengths ranging between $10B_0$ and 10^3B_0 (note that Vincke and Baye do not explicitly specify the z parity of the states they calculate; from an inspection of their basis function it follows, however, that the basis is restricted to function of even z parity). For a close comparison of our results to those of Vincke and Baye, we have calculated $E_e^{(b)}$ at the equilibrium distances R_e given by these authors. The results (including $E_e^{(b)}$ values for the $1\sigma_g$ state; cf. Fig. 7) are given in Table IV. For $B\leq20B_0$, our binding energies are seen to be consistently larger than those of Vincke and Baye. Starting with the orbitals of largest $|m|$ value, our results become gradually smaller than those of Ref. 40 for higher field strengths. From a variation of the internuclear distance about the values given in Table IV, no substantial improvement of

TABLE IV. Total binding energies $E_e^{(b)}$ of the lowest states of *even* z parity of the magnetically dressed H_2^+ system at $\theta=0$, calculated at the equilibrium internuclear distances R_e given by Vincke and Baye (Ref. 40).

B/B_0	m	Parity	R_e (a.u.)	$E_e^{(b)}$ (a.u.) Ref. 40	$E_e^{(b)}$ (a.u.) Present work
10	0	g	0.950	2.1673	2.1750
	−1	u	1.510	1.3431	1.3523
	−2	g	1.880	1.0653	1.0748
	−3	u	2.162	0.9135	0.9226
	−4	g	2.404	0.8141	0.8222
20	0	g	0.756	2.8192	2.8268
	−1	u	1.164	1.7958	1.8049
	−2	g	1.428	1.4369	1.4454
	−3	u	1.630	1.2382	1.2442
	−4	g	1.802	1.1069	1.1088
50	0	g	0.559	3.9804	3.9878
	−1	u	0.827	2.6120	2.6177
	−2	g	1.006	2.1126	2.1090
	−3	u	1.144	1.8317	1.8129
	−4	g	1.258	1.6446	1.6062
100	−0	g	0.446	5.1389	5.1446
	−1	u	0.645	3.4387	3.4274
	−2	g	0.778	2.8029	2.7550
	−3	u	0.881	2.4418	2.3486
	−4	g	0.971	2.1996	2.0599
200	0	g	0.357	6.5904	6.5845
500	0	g	0.269	9.0475	8.9234
1000	0	g	0.219	11.3847	10.8344

our binding energies is obtained. We expect, however, a considerable gain in binding energy from an individual optimization of the parameter n_{eff} for the different $|m|$ values.

C. Wave functions

The structure of the electronic wave functions of magnetically dressed molecular orbitals is intimately related to the effect which the magnetic field has on the binding properties of molecules, i.e., on binding energies and equilibrium internuclear distances. In order to illustrate this effect, we consider in the following a few examples of wave functions for the H_2^+ system at $\theta=0$.

Figure 9 shows the z dependence of the $1\sigma_g$ wave function along the internuclear line ($x\equiv y\equiv 0$). If the internuclear distance is kept fixed at 2.0 a.u. (this value is virtually identical to the zero-field internuclear distance), the wave function on the z axis is seen to become increasingly enhanced when the field strength increases. While the enhancement in the vicinity of the nuclear centers is responsible for the increase in binding energy (cf. Fig. 2), the field-induced accumulation of electron density between the centers causes an increased screening of the nuclear charges, which tends to lower the equilibrium internuclear distance (cf. Table III). The field-induced constriction of the $1\sigma_g$ wave function about the z axis becomes apparent from Fig. 10 in which the x dependence of the wave function for $y\equiv z\equiv 0$ is shown.

The z dependence of the $1\sigma_u$ wave function along the internuclear line is shown in Fig. 11 for $R=2.0$ a.u. While the field-induced enhancement of the wave func-

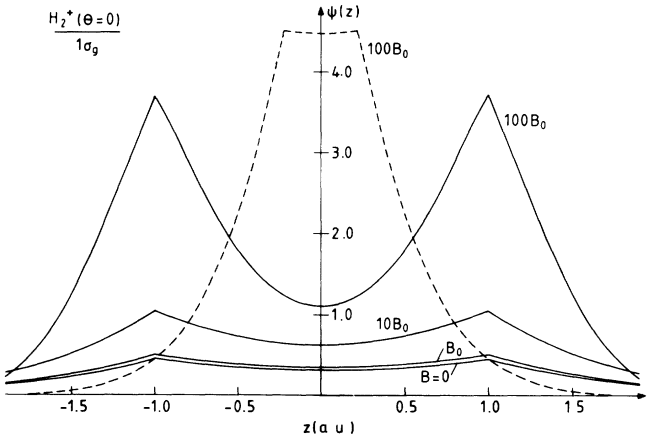

FIG. 9. Wave functions of the $1\sigma_g$ orbital of the magnetically dressed H_2^+ system at $\theta=0$, plotted along the z axis ($x\equiv y\equiv 0$) for various values of the field strength B. The solid curves refer to $R=2.0$ a.u., the dashed curve to the equilibrium internuclear distance at $B=100B_0$.

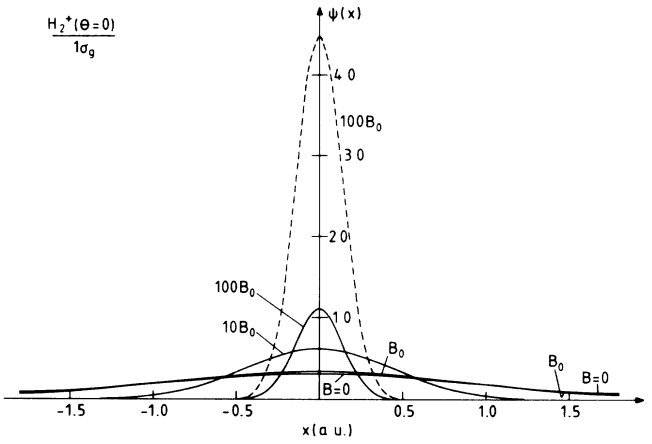

FIG. 10. Wave functions for the case of Fig. 9, plotted along the x axis ($y \equiv z \equiv 0$).

tion in the vicinity of the nuclear centers is about the same as that of the $1\sigma_g$ wave function, the requirement that the $1\sigma_u$ wave function has to vanish in the plane $z \equiv 0$ prevents the magnetic field from achieving a substantial accumulation of electron density between the centers. Accordingly, the effect of the field on the $1\sigma_u$ equilibrium internuclear distance is small: the very shallow minimum of the potential curve, which shows up roughly at $R = 12$ a.u. in the field-free case, remains shallow when the field strength increases. A field-induced shift of the minimum towards smaller R values is barely discernible in the range $B < B_0$. In Sec. V, we show that the effect of the field on the lowest ungerade state is much more pronounced when the field is oriented *perpendicular* to the internuclear axis.

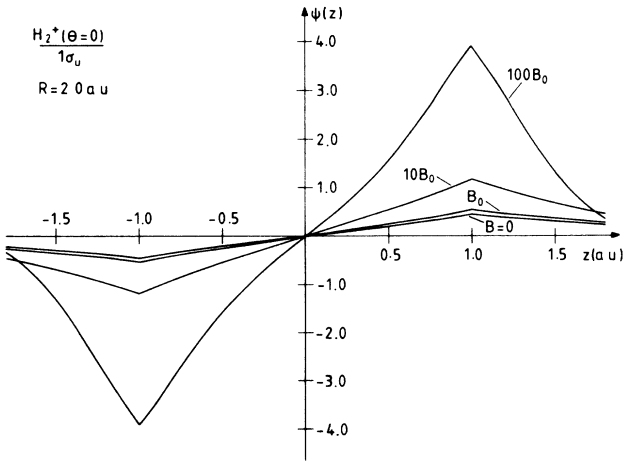

FIG. 11. Same as Fig. 9, for the $1\sigma_u$ orbital of the H_2^+ system. All curves refer to $R = 2.0$ a.u.

V. GENERAL PROPERTIES OF MAGNETICALLY DRESSED ONE-ELECTRON MOLECULAR ORBITALS: THE CASE OF ARBITRARY ANGLE θ

When the magnetic field is inclined with respect to the internuclear axis by an arbitrary, nonzero angle θ, the mixing of different m quantum numbers in the wave function leads, at a given level of accuracy, to a substantial increase of the basis size in comparison with the case $\theta = 0$. Correspondingly, if we confine the maximum basis size to about the same size as in the $\theta = 0$ calculation, we expect our method to provide accurate results only in a much more limited B range. To illustrate this point, we begin this section by considering explicitly, for a few typical examples, the m-mixing in magnetically dressed molecular orbitals.

A. m mixing in magnetically dressed molecular orbitals

Probabilities P_m for finding the component with good angular momentum projection m in the wave function of the lowest gerade orbital (1_g) of the dressed H_2^+ system are shown in Fig. 12 as a function of the angle θ. The 1_g orbital develops continuously from the $1\sigma_g$ orbital at $\theta = 0$ and merges into the 1_g^+ orbital at $\theta = 90°$ [the superscript $+$ or $-$ indicates the x parity of orbitals at $\theta = 90°$; cf. Eq. (11)].

At $B = B_0$ and $R = 2.0$ a.u., the admixture of $m \neq 0$ components in the 1_g wave function is seen to be about 2% at $\theta = 90°$. To achieve for these parameter values an accuracy in the 1_g orbital energy of better than 10^{-5} a.u., basis functions with $|m|$ values up to 4 have to be included in the expansion of the wave function (the probability $P_4 \equiv P_{-4}$ amounts to 0.3×10^{-4}). The admixture of $m \neq 0$ components increases rapidly with increasing internuclear distance R, as is seen from the results for $B = B_0$ and $R = 5.0$ a.u. shown in Fig. 12. In this case, an accuracy of better than 10^{-5} a.u. in the orbital energy

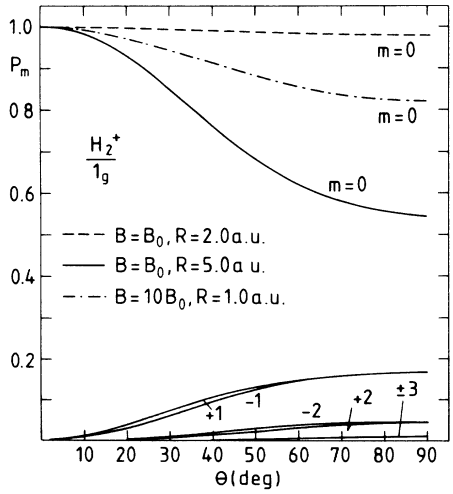

FIG. 12. Probabilities P_m to find the component with angular momentum projection m in the 1_g wave function of the magnetically dressed H_2^+ system, plotted as function of the angle θ for various values of field strength B and internuclear distance R.

is obtained if basis functions with $|m| \leq 7$ are kept in the expansion of the wave function. For $B = 10B_0$ and $R = 1.0$ a.u., the m mixing in the 1_g orbitals is substantially smaller than for $B = B_0$ and $R = 5.0$ a.u. The small m mixing in the 1_g orbital for small internuclear distances, which is observed even at $\theta = 90°$, reflects the strong binding of this orbital in the united-atom limit. This binding causes the magnetically dressed united-atom wave function to have (independent of the orientation of the field) large angular overlap with an $l = 0$ orbital.

The m mixing in higher orbitals is more involved than in the 1_g orbital. For large angles θ, the mixing is decisively influenced by the x parity assigned to the orbital in the limit $\theta = 90°$. For even x parity, the wave function is allowed to be nonzero on the internuclear axis and accordingly can have a nonvanishing $m = 0$ component; no such component is present in the wave function of an orbital having odd x parity. Whether an orbital develops, with increasing θ, into a + orbital or into a − orbital depends on the internuclear distance. For example, the $1\sigma_u$ orbital at $\theta = 0$ in the H_2^+ system develops into the 1_u^- orbital at $\theta = 90°$ if $R = 0$; for $R \to \infty$, the $1\sigma_u$ orbital develops into the 1_u^+ orbital (a discussion of the "correlations" of magnetically dressed molecular orbitals between the limits $\theta = 0$ and 90° will be given in Sec. V B).

Strong m mixing, even at very small angles θ, occurs in the vicinity of real crossings of orbitals of like parity, but with different m quantum numbers at $\theta = 0$. An example for this situation is the crossing of the $1\sigma_u$ and $1\pi_u$ ($m = -1$) orbitals at $R = 1.573$ a.u. in the H_2^+ system (cf. Figs. 2 and 14 below). For $\theta \neq 0$, the real crossing turns into an avoided crossing of the 1_u and 2_u orbitals which eventually, at $\theta = 90°$, merge in the 1_u^+ and 1_u^- orbitals.

In the calculations whose results are presented in the following subsections, we restricted the Hylleraas basis to functions with $|m| \leq 7$ and adjusted the maximum values of the labels n and l in such a way that the maximum dimension of the basis set was not larger than 530. For the parameter n_{eff}, the values obtained by minimizing the $1\sigma_g$ energy of the H_2^+ system at $\theta = 0$ were used throughout (cf. Fig. 8).

B. Molecular-orbital correlation diagrams

The dependence of the electronic orbital energies ε (as well as of the total energies $E = \varepsilon + Z_1 Z_2 / R$) on the parameters R and θ can, in principle, be visualized by representing the energy surfaces $\varepsilon(R,\theta)$ or $E(R,\theta)$ in the form of contour diagrams or projected "landscapes." It appears, however, that the amount of information contained in a complete energy surface is too large to be made visible in a single two-dimensional plot. We therefore resort to old-fashioned correlation diagrams showing the θ dependence of the energies at fixed R and B, or the R dependence at fixed θ and B.

In the correlation diagram of Fig. 13, the θ dependence of the electronic energies of the lowest gerade and ungerade orbitals of the dressed H_2^+ system is shown for $B = B_0$ and $R = 2.0$ a.u. The most interesting piece of information that can be gained from diagrams like this is the position of the minima of the energy curves [note Eq. (12b) and the relation $\varepsilon(-\theta) = \varepsilon(\theta)$]. These minima determine the equilibrium positions about which the magnetically dressed molecule may perform transverse vibrations.[43] According to Fig. 13, the equilibrium positions for $B = B_0$ and $R = 2.0$ a.u. are $\theta = 0$ for the 1_g and 2_u orbitals and $\theta = 90°$ for the 1_u and 2_g orbitals.

The behavior of the energy curves of Fig. 13 in the small-θ range can be elucidated in the following way.

Expanding the Hamiltonian (8) to order θ^2 about $\theta = 0$, one obtains

$$H(\theta) = H(\theta=0) + \theta \left[\frac{B}{2c} l_x - \frac{B^2}{4c^2} xz \right] - \theta^2 \left[\frac{B}{4c} l_z + \frac{B^2}{8c^2} (x^2 - z^2) \right] . \tag{26}$$

The corresponding energies, evaluated in second-order (nondegenerate) perturbation theory,[51] are

$$\varepsilon_i = \varepsilon_i^{(m)} + \theta^2 \left[-\frac{B}{4c} m + \frac{B^2}{4c^2} \left[\frac{\pi}{5} \right]^{1/2} Q_i^{(m)} + \sum_{m' \neq m} \sum_{i'=1,2\ldots} \frac{| \langle \psi_i^{(m)} | \frac{B}{2c} l_x - \frac{B^2}{4c^2} xz | \psi_{i'}^{(m')} \rangle |^2}{\varepsilon_i^{(m)} - \varepsilon_{i'}^{(m')}} \right] , \tag{27}$$

where $\varepsilon_i^{(m)}$ ($i = 1,2\ldots$) are the eigenvalues of $H(\theta = 0)$ (corresponding to given parity if $Z_1 = Z_2$), and $\psi_i^{(m)}$ the associated eigenfunctions. The quantity $Q_i^{(m)}$ is the electric quadrupole moment of $\psi_i^{(m)}$,

$$Q_i^{(m)} \equiv \langle \psi_i^{(m)} | r^2 Y_2^0 | \psi_i^{(m)} \rangle = -(5/4\pi)^{1/2} \langle \psi_i^{(m)} | x^2 - z^2 | \psi_i^{(m)} \rangle . \tag{28}$$

In the following, we refer to the first, second, and third terms in the square brackets of Eq. (27) as the (magnetic) dipole term, the (electric) quadrupole term, and the second-order term, respectively.

For the lowest of the gerade orbitals shown in Fig. 13, the 1_g orbital, the dipole term is zero and the second-order term negative. The rise of the 1_g energy curve therefore signals a positive quadrupole moment $Q_1^{(0)}$ at $B = B_0$ and $R = 2.0$ a.u. This result can be anticipated from the z and x dependence of the $1\sigma_g$ wave function shown in Figs. 9 and 10. From the behavior of the 1_u energy curve in Fig. 13, the sign of the $1\sigma_u$ quadrupole moment cannot be uniquely determined. It is likely, however, that the rather rapid decrease of the curve is caused

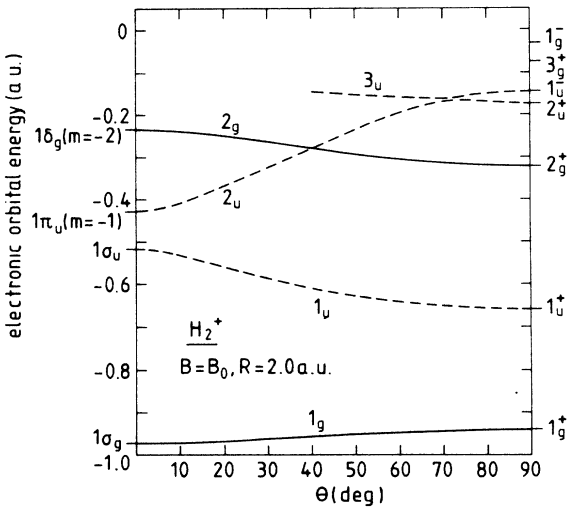

FIG. 13. Electronic energies of the lowest orbitals of the magnetically dressed H_2^+ system at $B=B_0$ and $R=2.0$ a.u., plotted as a function of the angle θ. Solid curves, "gerade" orbitals; dashed curves, "ungerade" orbitals.

mainly by the second-order term in Eq. (27), which must be negative anyhow and should be of fairly large magnitude because of the small $1\sigma_u - 1\pi_u(m=-1)$ energy difference. The positive $1\pi_u(m=-1)$ dipole term and a presumably large, positive second-order term make plausible the rapid rise of the 2_u energy curve in the small-θ range. Since the dipole term for the $1\delta_g(m=-2)$ orbital is positive, the decrease of the 2_g energy curve apparently reflects a large negative $1\delta_g$ quadrupole moment and/or a large negative second-order term.

The qualitative behavior of the energy curves in the vicinity of $\theta=0$ may, of course, change as function of B and R. At $B=B_0$, it turns out that the maximum-minimum properties of the orbitals shown in Fig. 13 do not change when R is varied between very small values and 10 a.u. (cf. also Fig. 15 below). In other cases, it has to be decided by explicit calculation whether or not $\theta=0$ is an equilibrium position of the magnetically dressed H_2^+ system.

The behavior of the energy curves in the vicinity of $\theta=90°$ is not as easy interpreted as that for $\theta=0$. Performing an expansion similar to Eq. (27), one sees that the correction to the energy at $\theta=90°$ involves, apart from a second-order term, expectation values of the operators l_x and x^2-z^2 in states of good x parity (and of good full parity if $Z_1=Z_2$). These expectation values can neither be evaluated in closed form nor be rewritten in terms of multipole moments.

The energy curves shown in Fig. 13 establish "correlations" between magnetically dressed molecular orbitals with the field parallel and perpendicular to the molecular axis, respectively, i.e., they connect in a continuous way an orbital at $\theta=0$ to an orbital at $\theta=90°$. As in the case of the usual correlations[49] between united-atom and separated-atom orbitals, one has to distinguish in the present case between "adiabatic" and "diabatic" correlations.

The adiabatic correlations are established by following the energy curves obtained from the complete diagonalization of the Hamiltonian (8) all the way from $\theta=0$ to $\theta=90°$ (the assignment of a definite x parity in the limit $\theta=90°$ is easily accomplished by comparing orbital energies and wave functions calculated in the full basis to the corresponding quantities calculated in the basis sets with even and odd x parity, respectively). For the case of Fig. 13, the adiabatic correlations can be schematically written as

$$1_g:\ 1\sigma_g \rightarrow 1_g^+ ,$$
$$2_u:\ 1\sigma_u \rightarrow 1_u^+ ,$$
$$1_u:\ 1\pi_u(m=-1) \rightarrow 2_u^+ ,$$
$$2_g:\ 1\delta(m=-2) \rightarrow 2_g^+ .$$

Since in the strictly adiabatic case, energy curves of one and the same spatial symmetry [parity is the only spatial symmetry of the Hamiltonian (8) for $0<\theta<90°$ and $Z_1=Z_2$] are not allowed to cross, the adiabatic correlations are solely decided by the ordering of the levels of a given symmetry in the limits $\theta=0$ and $\theta=90°$, i.e., the lowest gerade orbital at $\theta=0$ correlates to the lowest gerade orbital at $\theta=90°$, etc.

Diabatic energy curves are usually constructed[49] from adiabatic energy curves by ignoring the splitting of the latter curves at "close" avoided crossings. An example for such a crossing is the 2_u-3_u avoided crossing at $\theta\simeq 70°$. The small splitting at this crossing indicates that the 2_u and 3_u orbitals (which correlate adiabatically to the 2_u^+ and 1_u^- orbitals, respectively) have, at $\theta\simeq 70°$, already "almost pure" x parity. Ignoring the 2_u-3_u splitting, one may construct a diabatic energy curve connect-

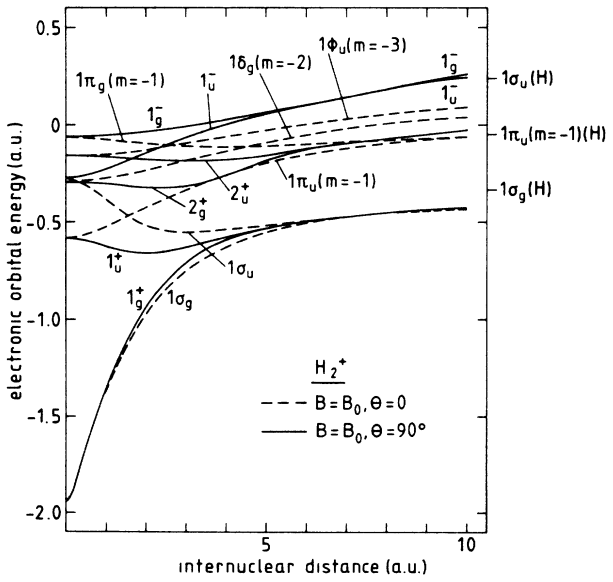

FIG. 14. Electronic energies of the lowest orbitals of the magnetically dressed H_2^+ system at $B=B_0$, plotted as function of internuclear distance for $\theta=0$ (dashed curves) and for $\theta=90°$ (solid curves), respectively. The separated-atom energies refer to the dressed H atom.

ing the $1\pi_u(m=-1)$ orbital at $\theta=0$ to the 1_u^- orbital at $\theta=90°$.

To illustrate further the effect of the magnetic field for nonzero angles θ, we display in Fig. 14 the R dependence of the energies of the lowest magnetically dressed H_2^+ orbitals at $\theta=90°$. Numerical values of these energies are given in Table V. Also shown in Fig. 14 are the energy curves of those $\theta=0$ orbitals which are degenerate with the $\theta=90°$ orbitals at $R=0$. It is evident that the degenerate orbitals can be transformed into each other by rotating the coordinate system through 90° about the y axis. Accordingly, the x parity of a $\theta=90°$ orbital at $R=0$ is identical to the z parity of the $\theta=0$ orbital with which it is degenerate; this rule is easily verified for the orbitals shown in Fig. 14.

The adiabatic correlations among the united-atom ($R=0$) and separated-atom ($R=\infty$) orbitals at $\theta=90°$ are governed by the conservation of x parity. In a symmetric system like H_2^+, pairs of energy curves of opposite parity and one and the same x parity correlate to a separated-atom orbital of just that x parity. In the strict separated-atom limit, the orbital energies are independent of the orientation of the magnetic field with respect to the internuclear axis (the only preferred direction in the separated-atom problem is the field direction), and the x parity of a $\theta=90°$ orbital agrees with the z parity of the

TABLE V. Energies (in a.u.) of the lowest orbitals of the magnetically dressed H_2^+ system at $B=B_0$ and $\theta=90°$, for different values of the internuclear distance R (in a.u.). For accuracy of the numbers, see text.

R	$\varepsilon_{1_g^+}$	$\varepsilon_{1_u^+}$	$\varepsilon_{2_g^+}$	$\varepsilon_{2_u^+}$	$\varepsilon_{1_g^-}$	$\varepsilon_{1_u^-}$
0.0	−1.9412	−0.5832	−0.2941	−0.1594	−0.0625	−0.2756
0.25	−1.833 85	−0.585 56	−0.294 63	−0.159 74	−0.061 01	−0.272 06
0.5	−1.659 02	−0.592 96	−0.296 47	−0.160 85	−0.059 89	−0.262 14
0.75	−1.492 90	−0.605 25	−0.299 44	−0.162 47	−0.058 03	−0.247 46
1.0	−1.347 67	−0.620 61	−0.303 41	−0.164 58	−0.055 41	−0.229 57
1.25	−1.222 53	−0.636 00	−0.318 14	−0.167 12	−0.052 03	−0.209 68
1.5	−1.114 52	−0.648 51	−0.313 27	−0.169 99	−0.047 88	−0.188 69
1.75	−1.020 84	−0.656 35	−0.318 28	−0.173 10	−0.042 96	−0.167 24
2.0	−0.939 28	−0.659 01	−0.322 51	−0.176 28	−0.037 28	−0.145 76
2.25	−0.868 23	−0.656 84	−0.325 21	−0.179 35	−0.030 88	−0.124 59
2.5	−0.806 52	−0.650 65	−0.325 61	−0.182 12	−0.023 80	−0.103 93
2.75	−0.753 31	−0.641 40	−0.323 05	−0.184 34	−0.016 12	−0.083 94
3.0	−0.707 91	−0.629 99	−0.317 05	−0.185 79	−0.007 91	−0.064 74
3.25	−0.669 68	−0.617 26	−0.307 43	−0.186 25	0.000 74	−0.046 38
3.5	−0.637 87	−0.603 87	−0.294 37	−0.185 57	0.009 76	−0.028 93
3.75	−0.611 60	−0.590 37	−0.278 43	−0.183 63	0.019 04	−0.012 39
4.0	−0.589 92	−0.577 15	−0.260 37	−0.180 40	0.028 53	0.003 23
4.25	−0.571 90	−0.564 49	−0.241 09	−0.175 91	0.038 14	0.017 93
4.5	−0.556 71	−0.552 56	−0.221 46	−0.170 29	0.047 82	0.031 75
4.75	−0.543 70	−0.541 46	−0.202 23	−0.163 72	0.057 52	0.044 74
5.0	−0.532 36	−0.531 18	−0.184 04	−0.156 42	0.067 21	0.057 00
5.25	−0.522 32	−0.521 73	−0.167 39	−0.148 62	0.076 87	0.068 59
5.5	−0.513 31	−0.513 03	−0.152 57	−0.140 54	0.086 48	0.079 64
5.75	−0.505 16	−0.505 03	−0.139 64	−0.132 40	0.096 04	0.090 26
6.0	−0.497 71	−0.497 65	−0.128 45	−0.124 35	0.105 58	0.100 57
6.25	−0.490 85	−0.490 83	−0.118 68	−0.116 52	0.115 10	0.110 65
6.5	−0.484 50	−0.484 50	−0.110 02	−0.108 98	0.124 62	0.120 61
6.75	−0.478 60	−0.478 60	−0.102 19	−0.101 74	0.134 19	0.130 50
7.0	−0.473 07	−0.473 07	−0.094 96	−0.094 82	0.143 82	0.140 37
7.25	−0.467 88	−0.467 88	−0.088 19	−0.088 20	0.153 53	0.150 28
7.5	−0.462 97	−0.462 98	−0.081 77	−0.081 84	0.163 37	0.160 24
7.75	−0.458 32	−0.458 32	−0.075 63	−0.075 71	0.173 33	0.170 27
8.0	−0.453 88	−0.453 89	−0.069 69	−0.069 78	0.183 44	0.180 37
8.25	−0.449 63	−0.449 63	−0.063 92	−0.064 00	0.193 71	0.190 52
8.5	−0.445 54	−0.445 54	−0.058 28	−0.058 35	0.204 12	0.200 64
8.75	−0.441 58	−0.441 58	−0.052 72	−0.052 80	0.214 67	0.210 60
9.0	−0.437 72	−0.437 73	−0.047 21	−0.047 30	0.225 28	0.220 10
9.25	−0.433 95	−0.433 96	−0.041 73	−0.041 84	0.235 85	0.228 69
9.5	−0.430 24	−0.430 26	−0.036 22	−0.036 38	0.245 99	0.236 15
9.75	−0.426 57	−0.426 60	−0.030 66	−0.030 89	0.254 65	0.242 71
10.0	−0.422 92	−0.422 97	−0.025 02	−0.025 33	0.261 30	0.248 68

orbital obtained by rotating the former orbital through 90° about the y axis of a coordinate system centered about the nucleus to which the orbital is attached. In the correlation diagram of Fig. 14, it is therefore sufficient to label the separated-atom orbitals by their m quantum number and parity. The lowest pair of "+" orbitals $(1_g^+, 1_u^+)$ correlates to the $1\sigma_g(H)$ orbital which has even z parity and, upon rotation through 90°, even x parity. Similarly, the pair $2_g^+, 2_u^+$ correlates to the $1\pi_u(m=-1)(H)$ orbital. The lowest pair of "−" orbitals $(1_u^-, 1_g^-)$ correlates to the $1\sigma_u(H)$ orbital which has odd z parity.

From Fig. 14 and from the numerical values of Table V, it is seen that the splitting of the 1_g^+ and 1_u^+ energy curves decreases, for large internuclear distances R, more rapidly with increasing R than does the $1\sigma_g$-$1\sigma_u$ splitting [note that for R values larger than the crossing distance 1.573 a.u. of the $1\sigma_u$ and $1\pi_u$ $(m=-1)$ orbitals, the 1_g^+ and 1_u^+ orbitals develop continuously from the $1\sigma_g$ and $1\sigma_u$ orbitals, respectively, when θ varies from 0 to 90°]. We shall discuss the reduced g-u splitting in the $\theta=90°$ orbitals in Sec. V C, in conjunction with a discussion of the behavior of the associated wave functions.

The departure of the 1_g^+ and 1_u^+ energy curves from the $1\sigma_g$ and $1\sigma_u$ curves in the range $R>7$ a.u. apparently reflects the gradual onset of inaccuracies in the absolute values of the orbital energies for $\theta=90°$. For $R\to\infty$, the energies are expected[52] to vary as $1/R$; such a variation is observed for the $1\sigma_g$ and $1\sigma_u$ curves in that R range where these orbitals are almost degenerate, but not for the 1_g^+ and 1_u^+ orbitals (cf. Tables I and V; note that the energies given in Table I are "exact" within the quoted accuracy).

Major inaccuracies in the large-R range are observed in the absolute energies of the 2_g^+ and 2_u^+ orbitals, which should converge monotonically towards the $1\pi_u(m=-1)(H)$ energy (we exclude here the possibility of avoided crossings of the 2_g^+ and 2_u^+ orbitals with higher orbitals in the range $R>10$ a.u., which might cause the 2_g^+ and 2_u^+ energy curves to decrease again in that range). From a mere inspection of Fig. 14, we estimate the 2_g^+ and 2_u^+ energies up to $R\simeq 6$ a.u. to be accurate to better than 10^{-2} a.u. The $2_g^+-2_u^+$ energy *difference* is clearly much more accurate; the monotonic decrease of this difference up to $R=7.25$ a.u. (cf. the numbers given in Table V) indicates an accuracy of better than 10^{-4} a.u. in this range. A considerably worse accuracy can be inferred for the 1_u^- and 1_g^- energies from their rapidly increasing splitting in the range $R>7.75$ a.u. The accuracy of the results shown in Fig. 14 can apparently be increased by individual optimization of the parameter n_{eff}.

C. Potential curves and equilibrium internuclear distances

In Fig. 15, total energies as function of internuclear distance (potential curves) are shown for the dressed H_2^+ system in the lowest g and u states at $B=B_0$, both for $\theta=0$ and $\theta=90°$, in comparison to the field-free energies. For the lowest g state, the minimum of the potential curve is seen to become more pronounced and its position

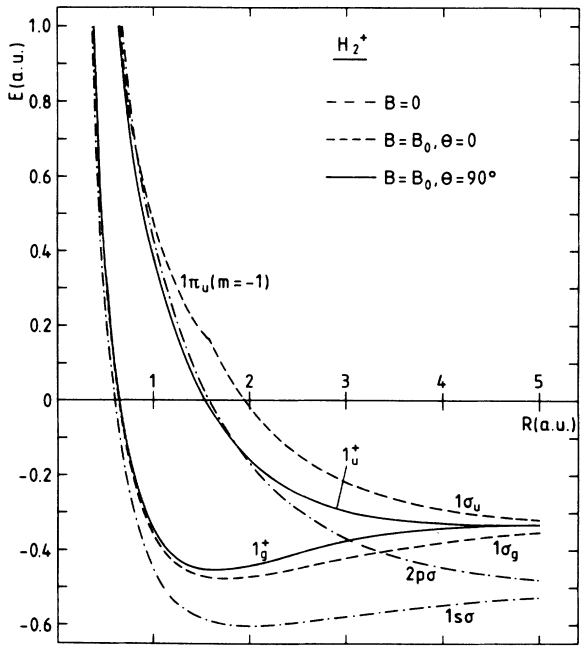

FIG. 15. Total energies E of the magnetically dressed H_2^+ system in its lowest electronic states, plotted as function of internuclear distance for $B=B_0$, $\theta=0$ and for $B=B_0$, $\theta=90°$. Curves pertaining to the field-free case are shown for comparison.

is seen to be shifted to a smaller R value when θ changes from 0 to 90°. Under this change, the potential curve of the lowest u state tends to become rather flat in the range $R\lesssim 5$ a.u. This feature indicates that the 1_u state (whose potential curve has a very shallow minimum at $R\simeq 12$ a.u. in the field-free case, which is not much affected by a magnetic field parallel to the internuclear axis, cf. Sec. IV C) possibly has a somewhat small equilibrium internuclear distance in a sufficiently strong field oriented *perpendicular* to the internuclear axis.

Figure 16 shows the B dependence of the equilibrium internuclear distance R_e for the dressed H_2^+ system in the 1_g^+ and 1_u^+ states at $\theta=90°$, in comparison with R_e-values for the $1\sigma_g$ state at $\theta=0$. Numerical values for R_e as well as for the total binding energies of the 1_g^+ and 1_u^+ states are given in Table VI. The equilibrium distance in the 1_g^+ state is seen to be consistently smaller than the corresponding distance in the $1\sigma_g$ state. For the 1_u^+ state beyond $B\simeq 5\times 10^5$ T, R_e values can be located which decrease rapidly with increasing B and possibly converge in the high-B limit towards the R_e values for the 1_g^+ state.

Our R_e values for the 1_g^+ state are in good agreement with those of Larsen[33] for $B\lesssim 10^2 B_0$. At $B=10^3 B_0$, Larsen's value is about 30% larger than the value we obtain by roughly extrapolating the values of Table VI. Our total binding energies for the 1_g^+ state agree well with those of Larsen for $B=B_0$ and $B=10B_0$. At $B=10^2 B_0$, our value is about 10% smaller than Larsen's value. Beyond 5×10^7 T, the slope of our 1_g^+ binding energy curve becomes negative. This effect apparently parallels

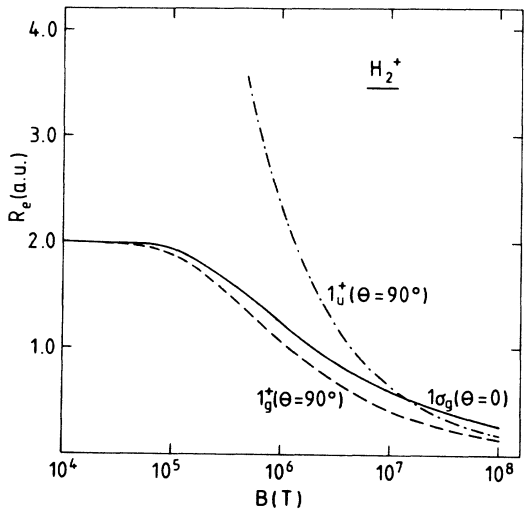

FIG. 16. Equilibrium internuclear distances R_e of the magnetically dressed H_2^+ system in the 1_g^+ and 1_u^+ states at $\theta=90°$, plotted as function of field strength B. R_e values for the $1\sigma_g$ state at $\theta=0$ are shown for comparison.

the behavior of the total binding energy of the $1\sigma_g$ state at $\theta=0$ in the range $B > 10^8$ T (cf. Fig. 7), which, by comparison with definitively more accurate calculations, has been identified as being caused by inaccuracies in our calculations. We therefore ascribe the departure of our results from those of Larsen in the range $B > 10^7$ T mainly to the inaccuracies of our results.

The accuracy of the equilibrium internuclear distances and total binding energies we have calculated for the 1_u^+ state is estimated to be of the same order as that for the 1_g^+ state. Accordingly, we assume the rapid decrease of the 1_u^+ equilibrium distance down to values smaller than the $1\sigma_g$ distance to be a real effect.

To complete the discussion of the total energies of the magnetically dressed H_2^+ system, we consider briefly the θ dependence of these energies at fixed R. This dependence determines the frequencies of small, transverse vibrations about equilibrium positions as well as the rotational properties of the molecule in the magnetic field.[43]

For the examples shown in Fig. 15, the total energy at arbitrary, fixed R changes montonically when θ varies between 0 and 90°. The energy minimum of the 1_g state is at $\theta=0$ throughout, the minimum of the 1_u state is at $\theta=90°$. The difference in total energy of the 1_g state at $\theta=90°$ and at $\theta=0$, i.e., the 1_g^+-$1\sigma_g$ energy difference (which is identical to the height of the potential barrier "seen" by the dressed molecule when it performs "hindered" rotations[43]), reflects the difference of the corresponding orbital energies (cf. Sec. V B), i.e., the potential barrier has zero height in the limits $R=0$ and ∞ and a maximum at $R \simeq 3$ a.u. A similar behavior is observed for the 1_u potential barrier height which reflects the $1\pi_u(m=-1)$-1_u^+ orbital energy difference in the R range below the $1\pi_u(m=-1)$-1_u^+ crossing, and the $1\sigma_u$-1_u^+ energy difference for R values larger than the crossing distance.

The θ dependence of the total energies of the 1_g and 1_u states at $B=B_0$ and $R=2.0$ a.u. is shown in Fig. 17. The results of the numerical calculation are compared to fit curves of the form $[E(90°)-E(0)]\times\sin^2\theta$. The good agreement between numerical result and fit curve for the 1_g state is a consequence of the small admixture of $m\neq 0$ components in the 1_g wave function (cf. Fig. 12), which entails the θ dependence of the energy to be dominated by the term proportional to $B^2\sin^2\theta$ in the Hamiltonian (8). The 1_u energy is less well fitted by the $\sin^2\theta$ curve, but can be shown[44] to be accurately approximated, at the given B and R values, if a $\sin^4\theta$ term is included in the fit function. In general, simple and accurate approximations to the θ dependence of the energy are highly useful since they may help to reduce the computing effort in studies of the rotational properties of magnetically dressed molecular system[43] and of electronic processes in field-affected ion-atom collisions.[44]

TABLE VI. Equilibrium internuclear distances R_e and total binding energies $E_e^{(b)}$ of the magnetically dressed H_2^+ system in the electronic 1_g^+ and 1_u^+ states at $\theta=90°$, for different values of the magnetic field strength B.

B	1_g^+		1_u^+	
(T)	R_e (a.u.)	$E_e^{(b)}$ (a.u.)	R_e (a.u.)	$E_e^{(b)}$ (a.u.)
0	1.997	0.602 64		
10^4	1.996	0.623 55		
2×10^4	1.991	0.643 75		
5×10^4	1.962	0.700 17		
10^5	1.879	0.781 92		
2×10^5	1.698	0.912 31		
5×10^5	1.343	1.1747	3.520	1.0402
10^6	1.067	1.4496	2.284	1.2965
2×10^6	0.826	1.7961	1.606	1.6158
5×10^6	0.575	2.3620	0.952	2.1135
10^7	0.428	2.8409	0.645	2.4930
2×10^7	0.313	3.2685	0.441	2.7497
5×10^7	0.204	3.3406	0.271	2.4080
10^8	0.148	2.2790	0.192	0.7717

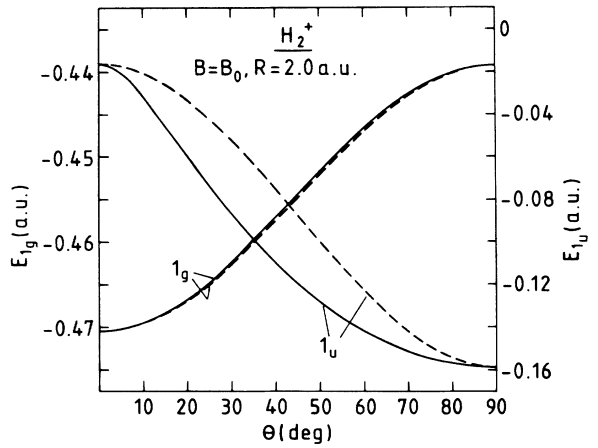

FIG. 17. Total energies of the magnetically dressed H_2^+ system in the 1_g and 1_u states at $B=B_0$ and $R=2.0$ a.u., plotted as function of the angle θ. Solid curves, result of numerical calculation. Dashed curves, fit curve assuming a $\sin^2\theta$ dependence of the energy.

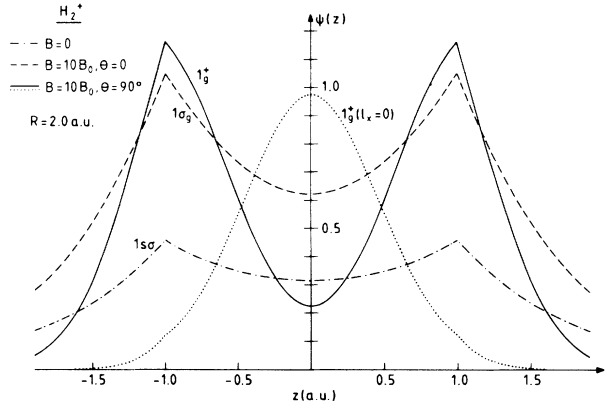

FIG. 18. Wave function of the 1_g^+ orbital of the magnetically dressed H_2^+ system at $B=10B_0$, $R=2.0$ a.u., $\theta=90°$, plotted along the z axis ($x\equiv y\equiv 0$). Solid curve, wave function corresponding to the full Hamiltonian (8); dotted curve, wave function corresponding to a Hamiltonian obtained from that of Eq. (8) by omitting the l_x term. The $1s\sigma$ wave function at $B=0$ and the $1\sigma_g$ wave function at $10B_0$, $\theta=0$ are shown for comparison.

D. Wave functions

To conclude the discussion of general properties of magnetically dressed molecular orbitals, we consider now the structure of the wave functions at $\theta=90°$ in comparison to that at $\theta=0$ and discuss the separation behavior of the dressed orbitals for large internuclear distances.

The z dependence of the 1_g wave function of the dressed H_2^+ system at $R=2.0$ a.u. and $B=10B_0$ is displayed in Fig. 18. The comparison of the $\theta=90°$ and $\theta=0$ wave functions reveals that the magnetic field, when rotated from parallel to perpendicular orientation with respect to the internuclear axis, tends to produce a localization of the wave function about the nuclear centers, with a corresponding decrease of the wave-function amplitude midway between the centers. This behavior apparently is nontrivial and requires same explanation.

Considering the Hamiltonian (8) at $\theta=90°$, one sees that the magnetic field gives rise to a two-dimensional oscillator term centered about the x axis as well as to an l_x term. One may argue now that the oscillator term will, for sufficiently large field strength, cause a compression of the wave function about the x axis. This view gets support from a plot of the z dependence of the total *static* potential $V(z)$ (i.e., the sum of two-center Coulomb potential and oscillator potential), as shown in Fig. 19. For $B=10B_0$, this potential exhibits a "pocket" midway between the nuclear centers. If it were not for the l_x term in the Hamiltonian, the wave function would become indeed localized in this pocket, as is seen from the dotted curve in Fig. 18, which has been calculated by "switching off" the l_x term. The comparison of the dotted curve with the solid curve in Fig. 18 reveals the crucial role which the l_x term plays for the localization properties of the wave function. In a sense, one may interpret the l_x term as a centrifugal term that causes the wave function to be pushed towards the nuclear centers.

The strong localization of the $\theta=90°$ wave functions about the nuclear centers at sufficiently large internuclear distances may be understood in a different way by considering the Hamiltonian (1) in the symmetric gauge centered on *one of the nuclei*. It follows from Eq. (6) that in this gauge the oscillator term in the $\theta=90°$ Hamiltonian is centered about an axis which is parallel to the x axis and passes through the nucleus on which the gauge is centered. The static potential $V(z)$ then no longer contains a pocket midway between the centers, and is not symmetric under the reflection $z\rightarrow -z$ [note also that the Hamiltonian no longer commutes with the full parity operator P when the center of gauge is located off the midpoint of the internuclear line, cf. the remark following Eq. (9)]. It is easily visualized that the potential ex-

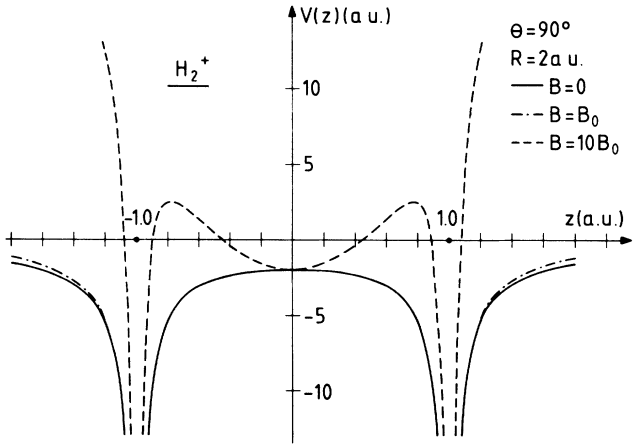

FIG. 19. Static potential V included in the Hamiltonian (8) for the magnetically dressed H_2^+ system at $\theta=90°$ and $R=2.0$ a.u., plotted along the z axis ($x\equiv y\equiv 0$) for $B=B_0$ and $B=10B_0$. The z dependence of the pure two-center Coulomb potential ($B=0$) is shown for comparison.

hibits a broad pocket centered about the gauge center and a narrow "chimneylike" pocket centered about the other nucleus. One might therefore argue that the wave function (and, accordingly, the density) is predominantly localized in the vicinity of the gauge center, in seeming contradiction to Fig. 18 which shows that the wave function is centered symmetrically about both centers. The resolution of this contradiction is apparently hidden in the action of the angular momentum operator l_s in Eq. (6), which serves to "distribute" the wave function in such a way about the centers that the gauge condition (7) is fulfilled, i.e., the wave function corresponding to the gauge centered on one of the nuclei differs from the function calculated in the *midpoint-centered gauge* only by a (plane-wave) phase factor. Thereby, it is guaranteed that the density remains invariant under a shift of the center of gauge.

The behavior of the z dependence of the 1_u wave function under a change of θ from 0 to 90°, as exemplified by the case of Fig. 20, is characterized by a more rapid decrease beyond the nuclear centers and a slight increase of the wave-function amplitude between the centers. This increase is apparently responsible for the tendency of the 1_u^+ state to exhibit a much smaller equilibrium internuclear distance than the $1\sigma_u$ state.

In order to illustrate the behavior of magnetically dressed molecular orbitals at large internuclear distances, we display in Fig. 21 the z dependence of the wave functions of the lowest H_2^+ orbitals at $B = B_0$ and $R = 5$ a.u. Considering the $\theta = 90°$ wave functions, one sees that in the range $|z| > 1.5$ a.u. the 1_g^+ and 1_u^+ functions are virtually identical in shape. This signals that the wave functions have attained almost complete separated-atom character in this range. The separated-atom character of the wave functions is reflected in the near degeneracy of the 1_g^+ and 1_u^+ orbitals (cf. Fig. 14). As can be anticipated from their fairly large energy splitting at $R = 5$ a.u. (cf. Fig. 14), the $1\sigma_g$ and $1\sigma_u$ wave functions at this R value still show some discrepancies in their shape even in the

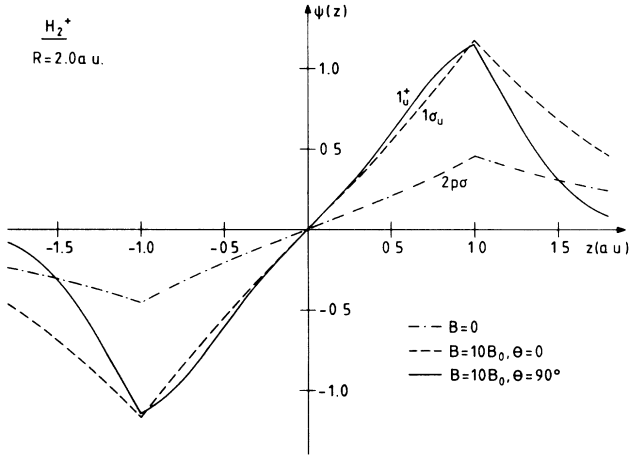

FIG. 20. Wave function of the 1_u^+ orbital of the magnetically dressed H_2^+ system at $B = 10B_0$, $R = 2.0$ a.u., $\theta = 90°$, plotted along the z axis ($x \equiv y \equiv 0$). The $2p\sigma$ wave function at $B = 0$ and the $1\sigma_u$ wave function at $B = 10B_0$, $\theta = 0$ are shown for comparison.

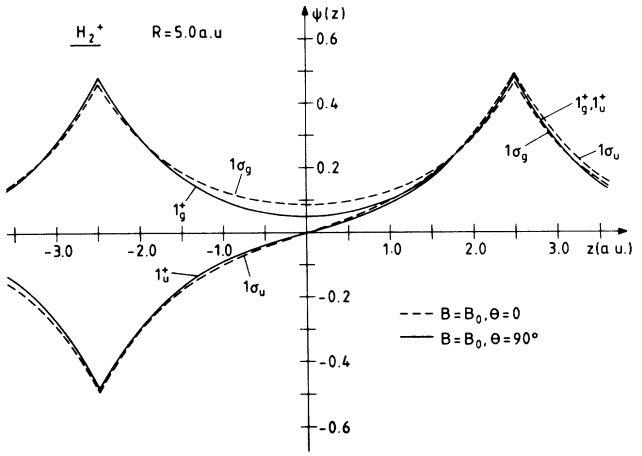

FIG. 21. Wave functions of the lowest "gerade" and "ungerade" orbitals of the magnetically dressed H_2^+ system at $B = B_0$ and $R = 5.0$ a.u., plotted along the z axis ($x \equiv y \equiv 0$) for $\theta = 0$ (dashed curves) and $\theta = 90°$ (solid curves).

vicinity of the nuclear centers. Nevertheless, one may infer from Fig. 21 that our method is able to describe properly the behavior of magnetically dressed molecular orbitals at large internuclear distances.

VI. SUMMARY AND CONCLUSIONS

In this paper, we have described and applied a general, flexible method for calculating "magnetically dressed" one-electron molecular orbitals. We have shown that this method, while being specifically adapted to the range of not-too-high magnetic fields, is capable of giving reliable results even at field strengths at which the magnetic interaction energy is by orders of magnitude larger than the Coulomb energy in the unperturbed molecular system. Particular emphasis has been placed in our investigation on the study of the dependence of the dressed orbitals on the angle between field direction and internuclear axis and on the study of the behavior of these orbitals at large internuclear distances. These studies are expected to form a point of departure for detailed investigations of the influence which strong magnetic fields have on electronic processes in quasimolecular ion-atom collisions and on the vibrational and rotational properties of molecules.

In obtaining the results presented here, we have not made any attempt to optimize the numerical procedure underlying our calculations. By employing more sophisticated methods for solving the generalized eigenvalue problem for the Hamiltonian matrix, it will be possible to achieve a considerable reduction of the computing time and to extend the calculations into parameter ranges not covered by the present results. A refined strategy for finding, at given values of the external parameters, optimum values for the parameters specifying the Hylleraas basis will be also helpful. In order to improve the convergence properties at large field strengths, one may, of course, think of augmenting the basis set by Landau orbitals aligned along the field direction. In this case, how-

ever, a closed-form evaluation of overlap and Hamiltonian matrix (which constitutes one of the major advantages of using the pure Hylleraas basis) will not be possible in general.

As long as we adhere to the framework of the present calculations, it will be advisable to restrict future applications of our method to the H_2^+ molecular ion and the quasimolecular H^+-H collision system in the range $B \leq B_0$. This range covers the field strengths estimated to be present in the vicinity of magnetized white-dwarf stars, and so it might be appropriate to envisage specific applications which are relevant to the physics of these objects.

APPENDIX: CLOSED-FORM EVALUATION OF THE ELEMENTS OF THE OVERLAP MATRIX AND OF THE HAMILTONIAN MATRIX

The elements of the overlap matrix $\underline{N}$,

$$N^{m,m'}_{nl,n'l'} = \langle \psi^m_{nl} \mid \psi^{m'}_{n'l'} \rangle \ , \tag{A1}$$

and of the Hamiltonian matrix $\underline{H}$,

$$H^{m,m'}_{nl,n'l'} = \langle \psi^m_{nl} \mid H \mid \psi^{m'}_{n'l'} \rangle \ , \tag{A2}$$

with the Hylleraas functions ψ^m_{nl} given by Eqs. (15) and the Hamiltonian H given by Eq. (8), can be expressed in terms of two types of basic integrals, $J_\alpha(n,n';m;a)$ and $K_\beta(l,l';m)$ involving the generalized Laguerre polynomials L_n^m and the associated Legendre functions P_l^m, respectively.

The integrals J_α are defined as

$$J_\alpha(n,n';m;a) = \int_1^\infty d\xi \exp\left[-\frac{\xi-1}{a}\right](\xi^2-1)^m \times \xi^\alpha L_n^m\left[\frac{\xi-1}{a}\right] L_{n'}^m\left[\frac{\xi-1}{a}\right] \tag{A3}$$

($\alpha = 0,1,2\ldots; m \geq 0$) and can be reduced, by introducing $\chi = (\xi-1)/a$ as a new integration variable, to

$$J_\alpha(n,n';m;a) = a^{2m+\alpha+1} \sum_{\mu=0}^{m} \binom{m}{\mu} \left[\frac{2}{a}\right]^\mu \sum_{\nu=0}^{\alpha} \binom{\alpha}{\nu} \left[\frac{1}{a}\right]^\nu \times I_{m-\mu+\alpha-\nu}(n,n';m) , \tag{A4}$$

where

$$I_\kappa(n,n';m) = \int_0^\infty d\chi \exp(-\chi)\chi^{m+\kappa} L_n^m(\chi) L_{n'}^m(\chi) \tag{A5}$$

($\kappa = 0,1,2\ldots$). A closed-form evaluation of the integrals I_κ is readily achieved by means of the recurrence relation

$$I_\kappa(n,n';m) = (2n'+m+1) I_{\kappa-1}(n,n';m) - (n'+m) I_{\kappa-1}(n,n'-1;m) - (n'+1) I_{\kappa-1}(n,n'+1;m) \tag{A6}$$

[$I_\kappa(n,n';m) = 0$ if $n' < 0$], which follows directly by inserting the recurrence relation[53]

$$\chi L_{n'}^m(\chi) = (2n'+m+1) L_{n'}^m(\chi) - (n'+m) L_{n'-1}^m(\chi) - (n'+1) L_{n'+1}^m(\chi) \tag{A7}$$

into Eq. (A5), and which allows I_κ for $\kappa \geq 1$ to be expressed in terms of

$$I_0(n,n';m) = \int_0^\infty d\chi \exp(-\chi)\chi^m L_n^m(\chi) L_{n'}^m(\chi) = \delta_{nn'} \frac{(n+m)!}{n!} \ . \tag{A8}$$

A necessary condition for the integrals I_κ to be nonzero is $\max\{n-\kappa,0\} \leq n' \leq n+\kappa$. The corresponding condition for the integrals J_α reads

$$\max\{n-m-\alpha,0\} \leq n' \leq n+m+\alpha \ . \tag{A9}$$

The symmetry of $I_\kappa(n,n';m)$ and $J_\alpha(n,n';m;a)$ with respect to an interchange of the indices n and n' is obvious.

The integrals K_β are defined as

$$K_\beta(l,l';m) = \int_{-1}^{+1} d\eta \, \eta^\beta P_l^m(\eta) P_{l'}^m(\eta) \tag{A10}$$

($\beta = 0,1,2\ldots; m \geq 0$). By means of the recurrence relation

$$K_\beta(l,l';m) = \frac{1}{2l'+1}[(l'-m+1)K_{\beta-1}(l,l'+1;m) + (l'+m)K_{\beta-1}(l,l'-1;m)] \tag{A11}$$

[$K_\beta(l,l';m) = 0$ if $l' < 0$], which follows by inserting the relation[53]

$$\eta P_{l'}^m(\eta) = \frac{1}{2l'+1}[(l'-m+1)P_{l'+1}^m(\eta) + (l'+m)P_{l'-1}^m(\eta)] \tag{A12}$$

into Eq. (A10), the integrals K_β for $\beta \geq 1$ can be expressed in terms of

$$K_0(l,l';m) = \int_{-1}^{+1} d\eta \, P_l^m(\eta) P_{l'}^m(\eta) = \delta_{ll'} \frac{2}{2l+1} \frac{(l+m)!}{(l-m)!} \ . \tag{A13}$$

The integrals K_β can be nonzero only if

$$\max\{l-\beta,0\} \leq l' \leq l+\beta \tag{A14a}$$

and

$$l+l'+\beta \ \text{ even} \ , \tag{A14b}$$

and are obviously symmetric with respect to an interchange of the indices l and l'.

Overlap matrix

Upon inserting the three-dimensional volume element $d\mathbf{r} = (R^3/8)(\xi^2-\eta^2)d\xi d\eta d\phi$ and performing the ϕ integration, the overlap matrix elements (A1) can be immediately written as

$$N^{m,m'}_{nl,n'l'} \equiv N^{m',m}_{n'l',nl} \equiv N^{-m,-m'}_{nl,n'l'} = \frac{R^3}{8}\delta_{mm'}[J_2(n')K_0(l)\delta_{ll'} - J_0(n')K_2(l')] , \tag{A15}$$

where we have introduced the shorthand notation $J_\alpha(n') \equiv J_\alpha(n,n';\mid m \mid;a)$ and $K_\beta(l') \equiv K_\beta(l,l';\mid m \mid)$. The selection rules for these matrix elements are

$$m' = m , \tag{A16a}$$

$$\max\{n - \mid m \mid -2,0\} \le n' \le n + \mid m \mid +2 , \tag{A16b}$$

$$\max\{l-2,0\} \le l' \le l+2 , \tag{A16c}$$

$$l + l' \text{ even} . \tag{A16d}$$

Hamiltonian matrix: Kinetic energy part

The operator of the kinetic energy $T = -\frac{1}{2}\nabla^2$ is expressed in terms of prolate spheroidal coordinates as

$$T = -\frac{2}{R^2(\xi^2-\eta^2)}\left[\frac{\partial}{\partial\xi}(\xi^2-1)\frac{\partial}{\partial\xi} + \frac{\partial}{\partial\eta}(1-\eta^2)\frac{\partial}{\partial\eta} + \left[\frac{1}{\xi^2-1} + \frac{1}{1-\eta^2}\right]\frac{\partial^2}{\partial\phi^2}\right] . \tag{A17}$$

When inserting this expression into the matrix element

$$T^{m,m'}_{nl,n'l'} = \langle \psi^m_{nl} \mid T \mid \psi^{m'}_{n'l'} \rangle , \tag{A18}$$

the denominator $\xi^2-\eta^2$ is seen to cancel out against the corresponding term in the volume element. After performing the ϕ integration, the differential equation[53] for the associated Legendre functions can be used to eliminate the η derivatives. The ξ derivative can be evaluated explicitly by using the relation[53]

$$\chi\frac{d}{d\chi}L^m_{n'}(\chi) = n'L^m_{n'}(\chi) - (n'+m)L^m_{n'-1}(\chi) . \tag{A19}$$

The resulting expression for the matrix elements of the kinetic energy operator reads

$$T^{m,m'}_{nl,n'l'} \equiv T^{m',m}_{n'l',nl} \equiv T^{-m,-m'}_{nl,n'l'} = \frac{R}{4}\delta_{mm'}\delta_{ll'}K_0(l)\left[\left[\frac{n'}{a} + \frac{1}{4a^2} + l(l+1) - (n'+m)(m+1)\right]J_0(n') + (n'+m)(m+1)J_0(n'-1) + \frac{1}{a}(n'+m+1)J_1(n') - \frac{1}{4a^2}J_2(n')\right] \tag{A20}$$

$[J_\alpha(n,n';m;a) = 0 \text{ if } n' < 0]$. The selection rules are

$$m' = m , \tag{A21a}$$

$$\max\{n - \mid m \mid -2,0\} \le n' \le n + \mid m \mid +2 , \tag{A21b}$$

$$l' = l . \tag{A21c}$$

Hamiltonian matrix: Potential-energy part

The potential-energy part $V = H - T$ of the Hamiltonian H can be decomposed into a sum of terms corresponding to different selection rules for the angular momentum projection m:

$$V = V^{\Delta m=0} + V^{\Delta m=\pm1} + V^{\Delta m=\pm2} \tag{A22}$$

$(\Delta m = m' - m)$, where

$$V^{\Delta m=0} = -\left[\frac{Z_1}{r_1} + \frac{Z_2}{r_2}\right] + \frac{B}{2c}\cos\theta\, l_z + \frac{B^2}{8c^2}\{(x^2+y^2) - \sin^2\theta([x^2]^{\Delta m=0} - z^2)\} , \tag{A23}$$

$$V^{\Delta m=\pm1} = \frac{B}{2c}\sin\theta\, l_x - \frac{B^2}{8c^2}\sin2\theta\, xz , \tag{A24}$$

$$V^{\Delta m=\pm2} = -\frac{B^2}{8c^2}\sin^2\theta[x^2]^{\Delta m=\pm2} , \tag{A25}$$

and

$$r_1 = \frac{R}{2}(\xi+\eta) , \tag{A26}$$

$$r_2 = \frac{R}{2}(\xi-\eta) , \tag{A27}$$

$$x=\frac{R}{2}[(\xi^2-1)(1-\eta^2)]^{1/2}\cos\phi\ , \tag{A28}$$

$$y=\frac{R}{2}[(\xi^2-1)(1-\eta^2)]^{1/2}\sin\phi\ , \tag{A29}$$

$$z=\frac{R}{2}\xi\eta\ , \tag{A30}$$

$$[x^2]^{\Delta m=0}=\frac{R^2}{8}(\xi^2-1)(1-\eta^2)\ , \tag{A31}$$

$$[x^2]^{\Delta m=\pm 2}=\frac{R^2}{8}(\xi^2-1)(1-\eta^2)\cos 2\phi\ , \tag{A32}$$

$$l_x=-i\frac{[(\xi^2-1)(1-\eta^2)]^{1/2}}{\xi^2-\eta^2}\left[\left[\xi\frac{\partial}{\partial\eta}-\eta\frac{\partial}{\partial\xi}\right]\sin\phi-\frac{\xi\eta(\xi^2-\eta^2)}{(\xi^2-1)(1-\eta^2)}\cos\phi\frac{\partial}{\partial\phi}\right]\ , \tag{A33}$$

$$l_z=-i\frac{\partial}{\partial\phi} \tag{A34}$$

(note that we have taken the midpoint of the internuclear line as the origin to which the Cartesian coordinates x,y,z refer). The matrix elements $V^{(0)m,m'}_{nl,n'l'}$ of $V^{\Delta m=0}$ are readily evaluated with the result

$$\begin{aligned}V^{(0)m,m'}_{nl,n'l'}\equiv V^{(0)m',m}_{n'l',nl}=\delta_{mm'}\Bigg[&-\frac{R^2}{4}[(Z_1+Z_2)J_1(n')K_0(l)\delta_{ll'}+(Z_2-Z_1)J_0(n')K_1(l')]\\&+\left[\frac{B}{2c}\cos\theta\, m-\frac{R^2}{4}\frac{B^2}{8c^2}(1-\tfrac{1}{2}\sin^2\theta)\right]N^{m,m'}_{nl,n'l'}\\&+\frac{R^5}{32}\frac{B^2}{8c^2}(1-\tfrac{1}{2}\sin^2\theta)[J_4(n')K_0(l)\delta_{ll'}-J_0(n')K_4(l')]\\&-\frac{R^5}{32}\frac{B^2}{8c^2}(1-\tfrac{3}{2}\sin^2\theta)[J_4(n')K_2(l')-J_2(n')K_4(l')]\Bigg]\ ,\end{aligned} \tag{A35}$$

the selection rules being

$$m'=m\ , \tag{A36a}$$

$$\max\{n-|m|-4,0\}\le n'\le n+|m|+4\ , \tag{A36b}$$

$$\max\{l-4,0\}\le l'\le l+4\ , \tag{A36c}$$

$$l+l'\ \text{ even, if } Z_1=Z_2\ . \tag{A36d}$$

In the evaluation of the matrix elements $V^{(1)m,m'}_{nl,n'l'}$ corresponding to the term $V^{\Delta m=\pm 1}$, the ξ and η derivatives appearing in the l_x operator can be performed by using Eq. (A19) and the relation[53]

$$(1-\eta^2)\frac{d}{d\eta}P^m_{l'}(\eta)=(l'+1)\eta P^m_{l'}(\eta)-(l'-m+1)P^m_{l'+1}(\eta)\ . \tag{A37}$$

The remaining integral as well as the integral involving the xz operator are easily transformed, by using the relations[53]

$$L^{m-1}_{n'}(\chi)=L^m_{n'}(\chi)-L^m_{n'-1}(\chi) \tag{A38}$$

and

$$(2l'+1)(1-\eta^2)^{1/2}P^{m-1}_{l'}(\eta)=P^m_{l'-1}(\eta)-P^m_{l'+1}(\eta)\ , \tag{A39}$$

into integrals which are diagonal in the quantum number m and which therefore can be expressed in terms of the integrals J_α and K_β. The result for the nonzero matrix elements of $V^{\Delta m=\pm 1}$ with $m\ge 1$ is

$$V^{(1)m,m-1}_{nl,n'l'}\equiv V^{(1)m-1,m}_{n'l',nl}=U^{(1)m,m-1}_{nl,n'l'}+W^{(1)m,m-1}_{nl,n'l'}\ , \tag{A40}$$

where

$$\begin{aligned}U^{(1)m,m-1}_{nl,n'l'}&=\frac{B}{2c}\sin\theta\,\langle\psi^m_{nl}\,|\,l_x\,|\,\psi^{m-1}_{n'l'}\rangle\\&=\frac{R^3}{16}\frac{B}{2c}\sin\theta\left[[J_1(n')-J_1(n'-1)]K_0(l)\delta_{ll'}-\frac{1}{2a(2l'+1)}[J_0(n')+J_0(n'-1)][K_1(l'-1)-K_1(l'+1)]\right]\end{aligned} \tag{A41}$$

and

$$W^{(1)m,m-1}_{nl,n'l'} = -\frac{B^2}{8c^2}\sin 2\theta \langle \psi^m_{nl} \mid xz \mid \psi^{m-1}_{n'l'} \rangle$$
$$= -\frac{R^5}{64}\frac{B^2}{8c^2}\sin 2\theta \frac{1}{2l'+1}\{[J_3(n')-J_3(n'-1)][K_1(l'-1)-K_1(l'+1)]$$
$$-[J_1(n')-J_1(n'-1)][K_3(l'-1)-K_3(l'+1)]\} . \quad \text{(A42)}$$

For $m \leq 0$, the nonzero matrix elements of $V^{\Delta m=\pm 1}$ are given by

$$V^{(1)-|m|,-(|m|+1)}_{nl,n'l'} \equiv V^{(1)-(|m|+1),-|m|}_{n'l',nl}$$
$$= U^{(1)|m|+1,|m|}_{n'l',nl} - W^{(1)|m|+1,|m|}_{n'l',nl} \quad \text{(A43)}$$

[note the phase convention inherent in Eq. (15b)]. The selection rules for the matrix elements $V^{(1)m,m'}_{nl,n'l'}$ are

$$m' = m \pm 1 , \quad \text{(A44a)}$$
$$\max\{n - |m| - 4, 0\} \leq n' \leq n + |m| + 4 , \quad \text{(A44b)}$$
$$\max\{l - 4, 0\} \leq l' \leq l + 4 , \quad \text{(A44c)}$$
$$l + l' \text{ even} . \quad \text{(A44d)}$$

Finally, the nonzero matrix elements of $V^{\Delta m=\pm 2}$ can be expressed, by repeated application of Eqs. (A38) and (A39), as

$$V^{(2)m,m-2}_{nl,n'l'} \equiv V^{(2)m-2,m}_{n'l',nl}$$
$$\equiv V^{(2)-m,-m+2}_{nl,n'l'} = -\frac{R^5}{128}\frac{B^2}{8c^2}\sin^2\theta \frac{1}{2l'+1}$$
$$\times \left\{[J_2(n')-2J_2(n'-1)+J_2(n'-2)]\right.$$
$$\times \left[\frac{1}{2l'-1}K_0(l+2)\delta_{l,l'-2} - \left(\frac{1}{2l'-1}+\frac{1}{2l'+3}\right)K_0(l)\delta_{ll'}\right.$$
$$\left. + \frac{1}{2l'+3}K_0(l-2)\delta_{l,l'+2}\right]$$
$$- [J_0(n')-2J_0(n'-1)+J_0(n'-2)]$$
$$\times \left.\left[\frac{1}{2l'-1}K_2(l'-2) - \left(\frac{1}{2l'-1}+\frac{1}{2l'+3}\right)K_2(l') + \frac{1}{2l'+3}K_2(l'+2)\right]\right\} \quad \text{(A45)}$$

for $|m| \neq 1$, and

$$V^{(2)1,-1}_{nl,n'l'} \equiv V^{(2)-1,1}_{n'l',nl} \equiv V^{(2)-1,1}_{nl,n'l'}$$
$$= \frac{R^5}{128}\frac{B^2}{8c^2}\sin^2\theta\{[J_4(n')-J_2(n')][K_0(l)\delta_{ll'}-K_2(l')]-[J_2(n')-J_0(n')][K_2(l')-K_4(l')]\} . \quad \text{(A46)}$$

The selection rules for the matrix elements $V^{(2)m,m'}_{nl,n'l'}$ are

$$m' = m \pm 2 , \quad \text{(A47a)}$$
$$\max\{n - |m| - 4, 0\} \leq n' \leq n + |m| + 4 , \quad \text{(A47b)}$$
$$\max\{l - 4, 0\} \leq l' \leq l + 4 , \quad \text{(A47c)}$$
$$l + l' \text{ even} . \quad \text{(A47d)}$$

The selection rules for the elements $H^{m,m'}_{nl,n'l'}$ of the complete Hamiltonian matrix follow from conditions (A21), (A36), (A44), and (A47):

$$m' = m, m \pm 1, m \pm 2 , \quad \text{(A48a)}$$
$$\max\{n - |m| - 4, 0\} \leq n' \leq n + |m| + 4 , \quad \text{(A48b)}$$

$$\max\{l-4,0\} \le l' \le l+4 \ , \tag{A48c}$$

$$l+l' \text{ even, if } Z_1 = Z_2 \ . \tag{A48d}$$

The case $\theta = 90°$

In the case $\theta = 90°$, the Hamiltonian matrix is diagonalized separately in the spaces $\{\psi_{nl}^{m=0}; \psi_{nl}^{m(+)}\}$ ("plus" space) and $\{\psi_{nl}^{m(-)}\}$ ("minus" space), respectively, where (for $m > 0$) the functions $\psi_{nl}^{m(\pm)}$ are defined by Eq. (16). The elements of the overlap matrix and of the Hamiltonian matrix referring to the plus and minus spaces can be immediately expressed in terms of the matrix elements corresponding to the basis functions ψ_{nl}^{m}. Except for one case, we have

$$\langle \psi_{nl}^{m(+)} \mid A \mid \psi_{n'l'}^{m'(+)} \rangle \equiv \langle \psi_{nl}^{m(-)} \mid A \mid \psi_{n'l'}^{m'(-)} \rangle \equiv \langle \psi_{nl}^{m} \mid A \mid \psi_{n'l'}^{m'} \rangle \ , \tag{A49}$$

where $A = 1$, T, $V^{\Delta m=0}$, $V^{\Delta m=\pm 1}$, or $V^{\Delta m=\pm 2}$. The exceptional case is that where $m = m' = 1$ and $A = V^{\Delta m=\pm 2}$, in which we have

$$\langle \psi_{nl}^{1(+)} \mid V^{\Delta m=\pm 2} \mid \psi_{n'l'}^{1(+)} \rangle \equiv -\langle \psi_{nl}^{1(-)} \mid V^{\Delta m=\pm 2} \mid \psi_{n'l'}^{1(-)} \rangle \equiv \langle \psi_{nl}^{1} \mid V^{\Delta m=\pm 2} \mid \psi_{n'l'}^{-1} \rangle \ . \tag{A50}$$

The matrix elements connecting the functions $\psi_{nl}^{m(+)}$ with the functions $\psi_{n'l'}^{m=0}$ are given by

$$\langle \psi_{nl}^{m(+)} \mid A \mid \psi_{n'l'}^{0} \rangle \equiv \langle \psi_{n'l'}^{0} \mid A \mid \psi_{nl}^{m(+)} \rangle = \sqrt{2} \langle \psi_{nl}^{m} \mid A \mid \psi_{n'l'}^{0} \rangle \ , \tag{A51}$$

where now $A = V^{\Delta m=\pm 1}$ or $V^{\Delta m=\pm 2}$.

[1] R. H. Garstang, Rep. Prog. Phys. **40**, 105 (1977).

[2] J. C. Gay, in *Progress in Atomic Spectroscopy, Part C*, edited by H. J. Beyer and H. Kleinpoppen (Plenum, New York, 1984), p. 177.

[3] M. Ruderman, in *Physics of Dense Matter*, edited by C. J. Hansen (Reidel, Dordrecht, 1974), p. 117.

[4] D. Moss, Phys. Rep. **140**, 1 (1986).

[5] Atomic and Molecular Physics Close to Ionization Thresholds in High Fields, edited by J. P. Connerade, J. C. Gay, and S. Liberman [J. Phys.Paris Colloq. **43**, C-2 (1982)].

[6] D. Kleppner, M. G. Littman, and M. L. Zimmerman, in *Rydberg States of Atoms and Molecules*, edited by R. F. Stebbings and F. B. Dunning (Cambridge University Press, Cambridge, England, 1983), p. 73.

[7] C. W. Clark, K. T. Lu, and A. F. Starace, in Ref. 2, p. 247.

[8] R. F. O'Connell, in Ref. 5, p. 81.

[9] *High Magnetic Fields in Semiconductors Physics*, Vol. 71 of *Springer Series in Solid-State Sciences*, edited by G. Landwehr (Springer-Verlag, Berlin, 1987).

[10] W. P. Reinhardt and D. Farrelly, in Ref. 5, p. 29.

[11] M. Robnik, in Ref. 5, p. 45.

[12] H. Friedrich and M. Chu, Phys. Rev. A **28**, 1423 (1983).

[13] C. Mega, H. Herold, W. Rösner, H. Ruder, and G. Wunner, Phys. Rev. A **30**, 1507 (1984).

[14] M. R. C. McDowell, in Ref. 5, p. 387.

[15] M. R. C. McDowell and M. Zarcone, Adv. At. Mol. Phys. **21**, 255 (1985).

[16] W. Rösner, G. Wunner, H. Herold, and H. Ruder, J. Phys. B **17**, 29 (1984).

[17] H. Forster, W. Strupat, W. Rösner, G. Wunner, H. Ruder, and H. Herold, J. Phys. B **17**, 1301 (1984).

[18] D. Wintgen and H. Friedrich, Phys. Rev. Lett. **57**, 571 (1986); Phys. Rev. A **35**, 1464 (1987).

[19] G. Wunner, U. Woelk, I. Zech, G. Zeller, T. Ertl, F. Geyer, W. Schweitzer, and H. Ruder, Phys. Rev. Lett. **57**, 3261 (1986).

[20] A. Holle, G. Wiebusch, J. Main, K. H. Welge, G. Zeller, G. Wunner, T. Ertl, and H. Ruder, Z. Phys. D **5**, 279 (1987).

[21] B. B. Kadomtsev and V. S. Kudryavtsev, Pis'ma Zh. Eksp. Teor. Fiz. **13**, 15 (1970) [JETP Lett. **13**, 9 (1971)]; Zh. Eksp. Teor. Fiz. **62**, 144 (1972) [Sov. Phys.—JETP **35**, 76 (1972)].

[22] C. P. de Melo, R. Ferreira, H. S. Brandi, and L. C. M. Miranda, Phys. Rev. Lett. **37**, 676 (1976).

[23] C. S. Lai and B. Suen, Can. J. Phys. **55**, 609 (1977).

[24] C. S. Lai, Can. J. Phys. **55**, 1013 (1977).

[25] R. K. Bhaduri, Y. Nogami, and C. S. Warke, Astrophys. J. **217**, 324 (1977).

[26] C. S. Warke and A. K. Dutta, Phys. Rev. A **16**, 1747 (1977).

[27] L. C. de Melo, T. K. Das, R. C. Ferreira, L. C. M. Miranda, and H. S. Brandi, Phys. Rev. A **18**, 12 (1978).

[28] M. Zaucer and A. Azman, Phys. Rev. A **18**, 1320 (1978).

[29] J. M. Peek and J. Katriel, Phys. Rev. A **21**, 413 (1980).

[30] M. S. Kaschiev, S. I. Vinitsky, and F. R. Vukajlovic, Phys. Rev. A **22**, 557 (1980).

[31] J. Ozaki and Y. Tomishima, J. Phys. Soc. Jpn. **49**, 1497 (1980); **52**, 1142 (1983).

[32] J. Ozaki and Y. Tomishima, Phys. Lett. **82A**, 449 (1981).

[33] D. M. Larsen, Phys. Rev. A **25**, 1295 (1982).

[34] G. Wunner, H. Herold, and H. Ruder, Phys. Lett. **88A**, 344 (1982).

[35] (a) A. V. Turbiner, Pis'ma Zh. Eksp. Teor. Fiz. **38**, 510 (1983) [JETP Lett. **83**, 618 (1983)]; (b) S. Basile, F. Trombetta, and G. Ferrante, Nuovo Cimento **9D**, 457 (1987).

[36] V. K. Khersonskij, Opt. Spektrosk. **55**, 825 (1983) [Opt. Spectrosc. (USSR) **55**, 495 (1983)].

[37] V. K. Khersonskij, Astron. Zh. **60**, 105 (1983) [Sov. Astron. **27**, 61 (1983)].

[38] J. C. LeGuillou and J. Zinn-Justin, Ann. Phys. (N.Y.) **154**, 440 (1984).

[39] V. K. Khersonskij, Astrophys. Space Sci. **98**, 255 (1984); **103**, 357 (1984); **117**, 47 (1985).

[40] M. Vincke and D. Baye, J. Phys. B **18**, 167 (1985).

[41] E. Hylleraas, Z. Phys. **71**, 739 (1931).

[42] U. Wille, in *Fundamental Processes in Atomic Collision Physics*, edited by H. Kleinpoppen, J. S. Briggs, and H. O. Lutz (Plenum, New York, 1985), p. 719.

[43] U. Wille, J. Phys. B **20**, L417 (1987).

[44] U. Wille, Phys. Lett. A **125**, 52 (1987).

[45] B. P. Carter, J. Math. Phys. **10**, 788 (1969).

[46] J. E. Avron, I. W. Herbst, and B. Simon, Ann. Phys. (N.Y.) **114**, 431 (1978).

[47] H. Herold, H. Ruder, and G. Wunner, J. Phys. B **14**, 751

(1981).
[48]D. Baye and M. Vincke, J. Phys. B **19**, 4051 (1986).
[49]U. Wille and R. Hippler, Phys. Rep. **132**, 129 (1986).
[50]P. Schmelcher and L. S. Cederbaum, Phys. Rev. A **37**, 672 (1988).
[51]L. Schiff, *Quantum Mechanics* (McGraw-Hill Kogakusha, Tokyo, 1968), Chap. 8.
[52]D. R. Bates and R. H. G. Reid, Adv. At. Mol. Phys. **4**, 13 (1968).
[53]*Handbook of Mathematical Functions,* edited by M. Abramowitz and I. A. Stegun (Dover, New York, 1965).